Petroleum Science 23 (2026) 608–625

Contents lists available at ScienceDirect

Petroleum Science

journal homepage: www.keaipublishing.com/en/journals/petroleum-science

Original Paper

Joint geostatistical seismic inversion of elastic and petrophysical properties using stochastic co-simulation models based on parametric copulas

Daniel Vázquez-Ramírez [a,*], Martín A. Díaz-Viera [b], Raúl del Valle-García [c]

[a] Department of Earth Sciences, School of Engineering, National Autonomous University of Mexico, Circuito de Posgrado S/N, Ciudad Universitaria, Coyoacan, 04510, Mexico City, Mexico
[b] Mexican Petroleum Institute, Eje Central Lazaro Cardenas No. 152, San Bartolo Atepehuacan, Gustavo A. Madero, 07730, Mexico City, Mexico
[c] Independent consultant, Mexico City, Mexico

ARTICLE INFO

Article history:
Received 25 September 2024
Received in revised form
16 September 2025
Accepted 28 October 2025
Available online 13 November 2025

Edited by Meng-Jiao Zhou

Keywords:
Geostatistical seismic inversion
Bayesian inference
Joint probability distribution function
Parametric copula
Petrophysical simulation
Seismic property simulation

ABSTRACT

Seismic properties play a fundamental role in the geological and petrophysical modeling of reservoirs due to their dependence on petrophysical properties. Most existing stochastic seismic inversion methods are based on Gaussian probability distribution functions and assume linear dependence. Examples include sequential Gaussian co-simulation (SGCS) and direct sequential simulation (DSS). In contrast, spatial stochastic co-simulation methods based on Bernstein copulas (BCCS) have recently been developed. These methods do not require a specific distribution type or linear dependence, thereby overcoming the limitations of traditional approaches.

In this context, we propose a novel approach for the joint seismic inversion of elastic and petrophysical properties using parametric copulas within a Bayesian inference framework. A joint probability distribution is constructed using well-scale petrophysical and elastic property data, fitted to parametric copula functions and treated as prior information. The model parameters are then updated *a posteriori* using petrophysical properties scaled by a moving window averaging method and seismic properties upscaled using the Backus averaging method. The resulting posterior model is used within the inversion process to generate elastic property realizations at the seismic scale.

The inverse problem is solved using a simulated annealing algorithm that minimizes a global objective function combining the root-mean-square (RMS) error between synthetic and observed seismic traces, and the semivariogram error between the simulated and target variogram models. For each elastic realization, a reflectivity series is computed and convolved with a seismic wavelet to generate a synthetic seismic trace. The best-fitting elastic realization is then used to simulate the corresponding petrophysical property using the same joint probability distribution.

The proposed method was applied to a deepwater reservoir case study to estimate total porosity and acoustic impedance at the seismic scale. Results demonstrate that the use of parametric copulas reduces computational cost and execution time while enabling effective integration of nonlinear dependencies. The synthetic traces exhibit RMS errors below 8%, validating the accuracy and robustness of the copula-based inversion framework.

1. Introduction

The prediction of seismic and petrophysical properties is a key challenge in the geological and petrophysical modeling workflow (Cosentino, 2001). To predict the spatial distribution of petrophysical properties at the seismic scale, it is first necessary to estimate the spatial distribution of elastic properties. These elastic

* Corresponding author.
E-mail address: danielgeofisico89@gmail.com (D. Vázquez-Ramírez).
Peer review under the responsibility of China University of Petroleum (Beijing).

https://doi.org/10.1016/j.petsci.2025.10.029

properties act as a bridge between seismic and petrophysical models, making it essential to establish a methodology that links them through an inverse modeling approach. The process of transforming seismic traces to estimate elastic and petrophysical properties is commonly known as seismic inversion. This technique is based on the concept of the inverse problem, which involves estimating model parameters from a set of observations. Typically, seismic inversion involves three main stages: (1) defining an objective function that quantifies the misfit between observed and simulated data, (2) optimizing this function, and (3) solving the resulting system of equations to obtain a quantitative model of subsurface properties. In this context, the forward model refers to the physical process that simulates seismic traces from elastic properties under specific assumptions, such as vertical incidence and horizontal layering. Traditional approaches to seismic inversion often rely on forward models formulated using convolutional or finite-difference approximations. The objective function evaluates how well these simulated traces match the observed seismic data and serves as the basis for guiding the inversion process through optimization. These are commonly optimized using criteria such as the L_1 norm or least squares, aiming to minimize the objective function and obtain the most probable solution. However, a major limitation of these approaches is their reliance on linearization, which can introduce uncertainty into the predictive model.

Seismic inversion in the petroleum industry has been an active area of research since the 1980s. Foundational studies by Oldenburg et al. (1983), Cooke and Schneider (1983), and Gelfand and Larner (1984) introduced linearized inversion techniques that utilized seismic surveys and well-log data, often optimizing objective functions based on maximum likelihood or the L_1 norm. Since the 1990s, geostatistical seismic inversion (GSI) methods have progressively evolved, integrating petrophysics, rock physics, and seismic data under Gaussian distribution assumptions, as demonstrated by the works of Bortoli et al. (1993), Haas and Dubrule (1994), Buland and Omre (2003), Dubrule et al. (2003), Doyen (2007), and Grana (2014). Unlike deterministic inversion approaches that yield a single best-fit model, GSI generates multiple equiprobable realizations that honor well-log information and spatial continuity through variogram modeling using the Sequential Gaussian Simulation method (Chilès and Delfiner, 2012). This allows for the quantification of subsurface uncertainty and provides a probabilistic framework for estimating elastic and petrophysical properties—making it highly suitable for reservoir characterization and risk analysis.

Several recent developments in geostatistical seismic inversion (GSI) have extended traditional Gaussian-based formulations toward non-linear, data-driven, and hybrid frameworks to capture fine-scale heterogeneity and characterize porosity and permeability distributions even at sub-seismic resolutions. For instance, Penna and Lupinacci (2024) applied a three-dimensional GSI workflow to model metric-scale flow units in Brazilian pre-salt carbonate reservoirs, emphasizing the value of sequential simulation and variogram constraints in facies-dependent petrophysical modeling. Similarly, Fernandes et al. (2024) combined GSI with Bayesian facies classification to improve porosity estimation and lithological discrimination in heterogeneous carbonate–igneous systems, demonstrating the effectiveness of integrating facies-related rock-physics models. de Figueiredo et al. (2025) introduced a Direct Multivariate Simulation (DMS) approach for non-linear and non-parametric rock-physics inversion, enabling the efficient generation of spatially correlated realizations that preserve heteroscedastic dependencies among variables. The DMS method extends traditional sequential simulation by employing a stepwise conditional transformation—a generalization of the normal-score and back-transformation procedures to multivariate non-Gaussian distributions—to generate realizations that strictly follow the empirical joint distribution of multiple variables. This framework allows the simulation of complex non-linear dependencies without assuming global Gaussianity, while maintaining spatial coherence among petrophysical and elastic properties. Despite these advances, many GSI techniques still rely on Gaussian or multi-Gaussian distributions (Azevedo and Soares, 2017; Pereira et al., 2020, 2023) or mixed-Gaussian models (Grana et al., 2017), which may be limited in representing complex, non-linear dependencies. To address such challenges, data-driven methods have also gained traction. For example, Zhang and Yang (2025) proposed a dual-learning network that directly inverts seismic attributes into reservoir properties, bypassing conventional forward modeling. While these neural approaches improve computational efficiency, they often require large training datasets and may lack physical interpretability. However, these approaches has notable disadvantages due to the limitations inherent to Gaussian simulations. For instance, Kriging equations are constrained to preserve low covariance between the original data and their estimates, and the variance of the random function is assumed to be stationary (Pyrcz and Deutsch, 2014). Moreover, these methods are not suitable when the number or spatial distribution of wells is insufficient, or when the measured of correlation (e.g., Pearson correlation) between petrophysical, seismic, and rock physics properties is too weak to support the linear dependence structure assumed by Gaussian-based models. In such cases, alternative methods capable of capturing nonlinear or weakly correlated dependencies such as copula-based approaches are more appropriate. To address these issues, alternative simulation techniques have been explored. Copula-based stochastic simulation is a promising alternative for simulating properties such as petrophysical or seismic attributes, given their conditional dependence. A key advantage of this approach is its flexibility: it offers a nonparametric technique that avoids assumptions about specific distribution function or dependence structures. In the geological-petrophysical modeling context, copula-based simulation enables the estimation of petrophysical and elastic models that are consistent with well-log statistics. As shown by Diaz-Viera et al. (2017), the resulting realizations do not exhibit artificial smoothing away from wells. This methodology improves GSI by reducing uncertainty. However, existing applications of copulas have primarily used nonparametric distribution functions, which—while accurate—require significant computational resources. To address this limitation, this work proposes the use of parametric copulas. These are simpler to implement within a Bayesian framework and require fewer computational resources, although they may sacrifice some accuracy compared to their nonparametric counterparts.

This work introduces a novel copula-based joint seismic inversion method, developed in response to the limitations of existing stochastic seismic inversion approaches. This is a significant constraint because it often requires transforming the data to satisfy distributional assumptions, potentially introducing bias during reverse transformation. To improve the simulation of the elastic property and reduce uncertainty compared to traditional approaches such as sequential Gaussian simulation, we define a joint probability distribution using a parametric copula. This distribution is fitted to geophysical well-log data describing petrophysical and elastic properties and subsequently updated using upscaled logs through a Bayesian inference framework. The resulting posterior model captures the joint dependence structure at the seismic scale and is used to generate elastic realizations within the inversion process.

The inverse problem is solved using the simulated annealing algorithm, which iteratively minimizes a global objective function. This objective function combines two terms: (1) the root-mean-square (RMS) error between synthetic and observed seismic traces, and (2) the semivariogram error between the variogram of the simulated elastic property and a target variogram derived from upscaled well-log data. Together, these components ensure that the resulting model honors both the seismic response and the spatial continuity observed in the wells. During optimization, the posterior model—estimated through the Bayesian copula framework—is used in the search function to generate realizations of the elastic property. For each candidate realization, a reflectivity series is computed and convolved with a seismic wavelet to produce a synthetic seismic trace. The misfit between this trace and the observed seismic data is evaluated using the objective function. The best-fitting elastic realization is then used as a conditioning variable to simulate the corresponding petrophysical property using the same joint probability distribution.

To demonstrate the theoretical framework and advantages of the proposed method, this paper is organized into eight sections. Section 1 presents the introduction, offering a concise overview of seismic inversion. Section 2 outlines the theoretical basis of the copula-based joint seismic inversion approach. Section 3 describes the application workflow, offering a detailed, step-by-step implementation guide. Section 4 presents the case study, including geological context, statistical analysis of well logs, dependence modeling, and variogram estimation. Section 5 provides a validation of the method using the seismic trace closest to the well. Section 6 details the inversion process using the nearest seismic inline, applying the parameters defined earlier. Section 7 discusses the results, and Section 8 presents the conclusions.

2. Parametric copula-based joint geostatistical seismic inversion method

GSI is a well-established approach for solving the inverse problem using a trace-by-trace scheme, as proposed by Bortoli et al. (1993) and Haas and Dubrule (1994). This type of inversion employs stochastic simulation to generate multiple realizations of an elastic property. These realizations are convolved with a wavelet to produce synthetic seismic traces, which are then compared to real seismic traces using an optimization method. The process iterates until a stopping criterion is satisfied, either based on the objective function or the maximum number of iterations.

The Copula-Based Joint Geostatistical Seismic Inversion Method integrates copula-based spatial stochastic co-simulation method to jointly simulate elastic and petrophysical properties. This method has been presented in several works by Diaz-Viera and Casar-González (2005), Diaz-Viera et al. (2006), Erdely and Díaz-Viera (2010), Hernández-Maldonado et al. (2012), Hernández-Maldonado et al. (2014), Erdely and Díaz-Viera (2015), Diaz-Viera et al. (2017), Vázquez-Ramírez (2018), Le et al. (2020) and Le (2021). Its main advantage lies in offering a nonparametric simulation approach through Bernstein Copula Co-simulation (BCCS), which eliminates the need to assume a specific marginal distribution or specific dependence structure. This method provides a robust alternative for simulating one property (e.g., elastic or petrophysical) conditioned on another, under a flexible dependence model. The resulting realizations are statistically consistent and preserve spatial distribution characteristics. Several studies, such as those by Bárdossy and Li (2008) and Gnann et al. (2018), have applied Gaussian copulas, which belong to the class of parametric copula models—these rely on multivariate normal distribution function to describe dependence structures. In contrast, nonparametric copula models offer greater flexibility by not assuming a predefined functional form, allowing them to capture more complex and potentially unknown dependence patterns. Despite their advantages, nonparametric copulas have not yet been applied to solve the geostatistical inverse problem.

The Bernstein Copula Co-simulation method is a procedure which can be basically subdivided into two steps:

- The joint probability distribution function is constructed using a dependency model based on the nonparametric Bernstein copula and the marginal distributions of the primary and secondary variables.
- A joint stochastic simulation of the primary variable conditioned by the secondary variable is performed in a global optimization framework using the simulated annealing method, where the objective function consists of the joint probability distribution function and the variogram model of the primary variable.

However, prior studies that apply this method to predict petrophysical properties at the seismic scale often follow a deterministic scheme. They typically subsample geophysical well-log data and rely on elastic property images, which may increase uncertainty. This is because the dependence model derived at the well scale can differ significantly from that obtained using upscaled or subsampled logs. To address this issue, parametric copula co-simulation (PCCS) is proposed as an alternative to BCCS. The use of parametric functions facilitates lower computational cost while maintaining modeling flexibility (Vázquez-Ramírez et al., 2023).

The Parametric Copula-Based Joint Geostatistical Seismic Inversion Method involves the following three main steps:

- Estimate the joint probability distribution model is estimated using a parametric copula, rather than a nonparametric Bernstein copula, within a Bayesian inference framework (see Appendix B).
- Generate realizations of the elastic property using its spatial dependence structure (variogram) until the synthetic trace with the lowest mean square error, relative to the observed seismic trace, is found—using the PCCS method.
- Predict the petrophysical property conditioned on the elastic property obtained in the previous step, using the same PCCS method.

The key innovation in this work is the use of Bayesian inference to update the dependence model, as demonstrated in the works by Kohn et al. (2006), Silva and Lopes (2008), Ausin and Lopes (2010), Min and Czado (2010) and Smith (2011). This approach allows the joint posterior probability distribution function to be updated using upscaled and/or subsampled well-log data, ensuring consistency with all available information sources. Because the dependence model can incorporate multiple elastic and petrophysical properties estimated from well logs, it enables the joint generation of realizations for these properties.

As part of the inversion procedure, joint realizations of petrophysical properties (e.g., porosity) and elastic properties (e.g., acoustic impedance) are generated. The simulated acoustic impedance is convolved with a wavelet to produce synthetic seismic traces, which are optimized using the global heuristic method of Simulated Annealing.

The theoretical framework described above serves as the foundation for the practical implementation of the inversion method. In the following section, we describe a detailed workflow that operationalizes this approach, from exploratory data analysis

to the generation of synthetic traces and petrophysical property simulation.

3. Joint geostatistical seismic inversion based on copulas workflow

The joint geostatistical seismic inversion method based on copulas is developed through the execution of seven steps, as illustrated in Fig. 1. The following subsections provide a detailed explanation of each step and the requirements for their implementation.

3.1. Exploratory data analysis

This step involves univariate and bivariate analysis of well logs and their upscaled versions. The univariate analysis includes the computation of descriptive statistics (e.g., minimum and maximum values), as well as the generation of histograms and boxplots to assess the impact of upscaling. The bivariate analysis

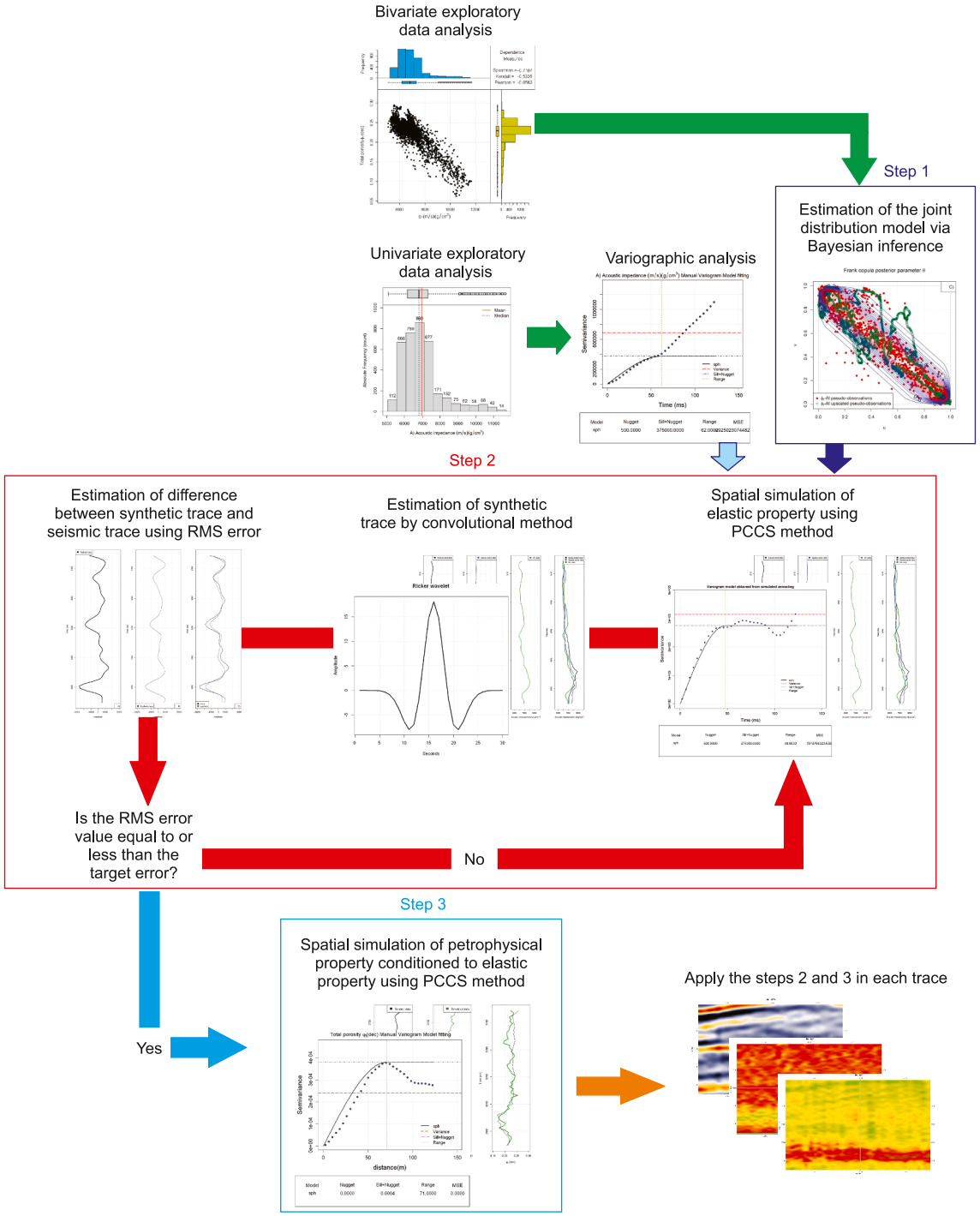

Fig. 1. Proposed workflow using co-simulation models based on parametric copulas for joint seismic inversion of elastic and petrophysical properties.

entails evaluating dependence measures and visualizing scatterplots before and after upscaling, to detect potential changes in relationships between variables.

3.2. Variographic analysis

This step consists of estimating and modeling the spatial correlation function (variogram) (Díaz-Viera, 2002) from the upscaled samples. The variogram model should be fitted to samples in the time domain, which facilitates the integration of seismic-scale realizations. Preprocessing is required to eliminate trends, and cross-validation should be employed to validate the chosen variogram model.

3.3. Estimation of the joint distribution model via Bayesian inference

The estimation of a joint probability distribution model between petrophysical and elastic properties is a key preparatory step in the proposed inversion framework. This step, corresponding to Step 1 in Fig. 1, defines the statistical dependence structure required to perform stochastic simulations. The model is constructed using a parametric copula function, which allows flexible modeling of nonlinear and asymmetric dependencies, and is calibrated using well-log data.

A Bayesian inference framework is used to estimate the parameters of both the marginal distributions and the copula model. The resulting posterior joint distribution model forms the basis for subsequent steps in the inversion workflow, including the simulation of elastic properties (Step 2) and the conditional simulation of petrophysical properties (Step 3). This modular structure ensures that the dependence model remains consistent throughout the inversion process and improves the robustness of the final estimates.

3.3.1. Prior information

Each marginal variable, X_1 and X_2, representing the elastic and petrophysical properties respectively, is independently fitted to several candidate parametric distributions. The marginal probability density functions $f_1(x_1;\ \alpha_1)$ and $f_2(x_2;\ \alpha_2)$, where x_i is the random variable and α is the parameter vector of the corresponding distribution, are selected based on maximum log-likelihood, as well as model selection criteria such as the Akaike Information Criterion (AIC; Hofert et al., 2019) and the Bayesian Information Criterion (BIC; Claeskens and Hjort, 2008). These criteria are briefly explained in Appendix D. Visual diagnostics such as histograms and cumulative distribution functions support the final selection.

Once the marginals are defined, a parametric bivariate copula with parameter θ is used to model the dependence between X_1 and X_2. The resulting joint prior distribution over the parameters is:

$$\pi(\theta,\alpha_1,\alpha_2)=\pi(\theta)\cdot\pi(\alpha_1)\cdot\pi(\alpha_2), \tag{1}$$

where $\pi(\alpha_1)$, $\pi(\alpha_2)$, and $\pi(\theta)$ are the prior distributions of the respective parameters.

3.3.2. Posterior model and likelihood function

The likelihood function is defined as the product of the copula density and the marginal densities evaluated at each observed pair $(x_1^{(j)},x_2^{(j)})$, for $j=1,\ldots,n$. The univariate margins are computed as $u=F_1(x_1^{(j)};\alpha_1)$ and $v=F_2(x_2^{(j)};\alpha_2)$, where F_1 and F_2 are the marginal cumulative distribution functions of the elastic and petrophysical properties, respectively.

To simplify computation and improve numerical stability, the log-likelihood form is used. The resulting log-posterior is:

$$\log(\pi(\theta,\alpha_1,\alpha_2|x_1,x_2))\propto\log(\pi(\theta))+\log(\pi(\alpha_1))+\log(\pi(\alpha_2))+\sum_{j=1}^{n}\log(c(u,v;\theta))+\sum_{j=1}^{n}\log f_1\left(x_1^{(j)};\alpha_1\right)+\sum_{j=1}^{n}\log f_2\left(x_2^{(j)};\alpha_2\right), \tag{2}$$

where $c(u, v; \theta)$ is the bivariate copula density function, and f_1, f_2 are the marginal probability density functions. A full explanation of this modeling framework and the general form of the likelihood function is provided in Appendix B.

The parameter vector $(\theta, \alpha_1, \alpha_2)$ is estimated using the Random Walk Metropolis-Hastings algorithm. After the initial estimation based on upscaled data, a second Bayesian update is performed using subsampled data as prior information. This two-stage inference acts as a quality control step, ensuring that the final model honors both well-scale statistics and seismic resolution constraints.

The resulting bivariate distribution function is used to generate synthetic samples during the inversion process. It is important to distinguish that the posterior model describes the probabilistic structure of the input variables, while the inversion algorithm uses an objective function that evaluates how well synthetic seismic traces match the observed data.

This model serves as the basis for generating elastic property realizations using the PCCS method. These realizations are evaluated using a hybrid objective function that balances spatial structure via variogram error and amplitude fidelity via RMS error. While the posterior model is estimated using Bayesian inference, the inversion itself is driven by a simulated annealing algorithm that minimizes this geostatistical–seismic misfit. This decoupling ensures that the statistical relationships learned from the input data are preserved, while still honoring the seismic response.

3.4. Spatial simulation of the elastic property using the PCCS method

To generate the synthetic trace that best matches the seismic trace, elastic properties are simulated using the Simulated Annealing method, which relies on two main components: the objective function and the search function.

The objective function includes the terms to be minimized. When it comprises multiple components, their contributions should be normalized to ensure a balanced optimization process. Deutsch and Journel (1998) recommended generating a few realizations for each individual term to assess their convergence behavior. In the global objective function, both the semivariogram error and the RMS are considered. The first objective function (Eq. (3) computes the semivariogram error:

$$O=\sum_h\frac{[\gamma^*(h)-\gamma(h)]^2}{\gamma(h)^2} \tag{3}$$

where $\gamma^*(h)$ is the semivariogram of the perturbed elastic property and $\gamma(h)$ is the model variogram.

To generate realizations of the elastic property and subsequently estimate $\gamma^*(h)$, the search function within the simulated annealing algorithm introduces perturbations to the initial elastic property image as follows:

- Propose an initial image.
- Randomly select a position in the image.
- Generate a candidate elastic value from the posterior joint distribution model estimated in Section 3.3.
- Accept the sample if its value lies within the observed range; otherwise, resample.
- Insert the new value into the selected position to generate a perturbed image, which is evaluated using Eq. (3).

This process is repeated until a maximum number of iterations is reached or the objective function reaches its minimum value.

3.5. Estimation of the synthetic trace using the convolutional model

The convolutional model is used to compute the synthetic seismic trace from the perturbed elastic property. First, the reflectivity series is computed by evaluating the P-wave reflection coefficient at normal incidence, r_t, as a function of the acoustic impedance contrast between two adjacent layers. The reflectivity series is calculated using Eq. (4):

$$r_t = \frac{(\rho_2)(V_{p2}) - (\rho_1)(V_{p1})}{(\rho_2)(V_{p2}) + (\rho_1)(V_{p1})} = \frac{AI_2 - AI_1}{AI_2 + AI_1} \tag{4}$$

where ρ_1 and V_{p1} are the density and P-wave velocity of the upper layer, and ρ_2 and V_{p2} are those of the lower layer; the acoustic impedances are defined as $AI_1 = \rho_1 \cdot V_{p1}$ and $AI_2 = \rho_2 \cdot V_{p1}$.

Then, the synthetic trace is obtained by convolving the reflectivity series r_t (Eq. (4)) with a wavelet f_t, which is estimated from the dominant frequency of the seismic image:

$$S_{st} = f_t * r_t \tag{5}$$

3.6. Estimation of the difference between the synthetic and real seismic traces using RMS error

The second objective function is the RMS error between the real and synthetic traces. If the RMS error is smaller than in the previous iteration, the proposal is accepted. Otherwise, a new realization of the elastic property must be generated.

3.7. Spatial simulation of the petrophysical property conditional on the elastic property using the PCCS method

After estimating the elastic property through seismic inversion process (Step 2), the petrophysical property is subsequently simulated. This step also employs the Simulated Annealing method, guided by the same posterior joint distribution model introduced in Section 3.3, ensuring statistical consistency between both attributes. The variogram model for the petrophysical property is derived from the subsampled well logs in the time domain. During the optimization, the posterior joint distribution is used within the search function to generate candidate realizations of the petrophysical property, which are conditioned to the elastic property obtained in the inversion step.

4. Case study description

4.1. Data description

To implement the stochastic simulation using parametric copulas, geophysical well logs were obtained from a deepwater well drilled in the Gulf of Mexico. This well penetrates the Miocene turbidite system, a significant unit due to the presence of unassociated hydrocarbon fields. The Miocene is subdivided into Lower, Middle, and Upper intervals. This study focuses on the Lower Miocene, where flow direction is primarily from southwest to northeast, with dominant channel systems. The lithology consists of medium-grained sandstones with evidence of volcanic material, feldspars, quartz, and metamorphic fragments. The rock is poorly consolidated and mineralogically immature, with reported porosity values ranging from 12% to 28% (Arreguin-Lopez et al., 2011).

The well used in this study was selected based on the quality and completeness of its available data. It is the most informative well in the study area, containing interpreted logs for acoustic impedance and total porosity, along with other petrophysical properties. Its depth coverage, vertical resolution, and the availability of well-established interpretations make it representative of the stratigraphic interval targeted in this work and suitable for validating the proposed inversion methodology.

The interval analyzed spans from 3035 to 3404.5 m, with a sampling interval of 0.1 m. The available well logs are acoustic impedance (AI) and total porosity (ϕ_t), as shown in Fig. 2. These logs were upscaled using two methods: total porosity was upscaled using the moving average technique, while acoustic impedance was upscaled using the Backus method based on V_p (P-wave velocity) and ρ (density) logs. Both methods apply a vertical seismic resolution of 28.44 m. Subsampled AI and ϕ_t values were extracted by computing the median within a ± 2 ms interval around each seismic grid node.

To predict the seismic attribute that best reproduces the observed seismic trace via convolution, the wavelet must be estimated. The wavelet is selected based on the dominant frequency observed in the amplitude spectrum of the inline seismic section closest to the well. As shown in Fig. 3, the dominant frequency is 20.16 Hz. In the absence of information about the seismic source type, a Ricker wavelet with a frequency of 20.16 Hz and a 4-ms sampling interval is used.

4.2. Exploratory data analysis from well logs

Descriptive statistics for the well, upscaled, and subsampled logs are provided in Table 1. The well and upscaled logs contain 3696 observations, while the subsampled log has 63 observations. For total porosity ϕ_t at the well scale, the difference between the mean and median is -0.008, with most outliers appearing on the left side of the histogram (Fig. 4(b)). In contrast, the AI log has a larger difference between the mean and median is 158.726, indicating positive skewness due to high-value outliers (Fig. 4(a)).

The upscaled total porosity values range from 0.165 to 0.261, and the histogram in Fig. 4D is visually similar to that of the well-scale data. The upscaled AI values range from 5835.096 to 8891.212 $(m/s)\cdot(g/cm^3)$ and display apparent bimodal behavior in Fig. 4(c). Subsampled AI values range from 5919.722 to 8539.996, indicating a reduction of approximately 2500 $(m/s)\cdot(g/cm^3)$ compared to the well-scale log. Subsampled ϕ_t values range from 0.167 to 0.257, with mean and median values similar to those of the original ϕ_t well log.

The dependence measures and corresponding scatterplots for (AI, ϕ_t) are presented in Table 2 and Fig. 5. At the well scale, the Spearman, Kendall, and Pearson coefficients are -0.7107, -0.5335, and -0.8563, respectively. After upscaling and subsampling, the dependence measures increase, particularly for Spearman and Kendall, which increase by approximately 0.2. However, the differences between the upscaled and subsampled cases remain small, less than 0.1, suggesting that the overall dependence structure remains stable despite changes in the univariate statistics.

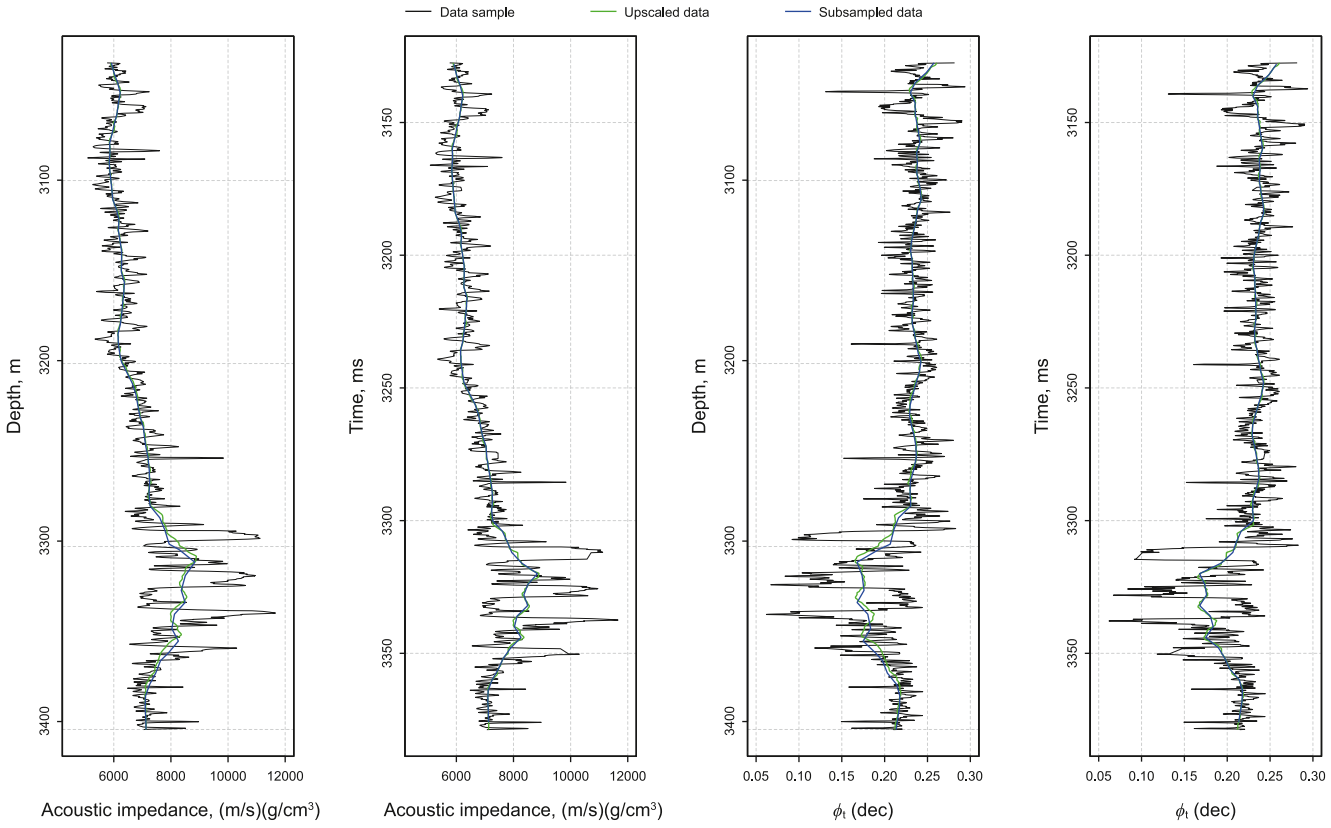

Fig. 2. Acoustic impedance (left) and total porosity ϕ_t (right) in depth and time domains.

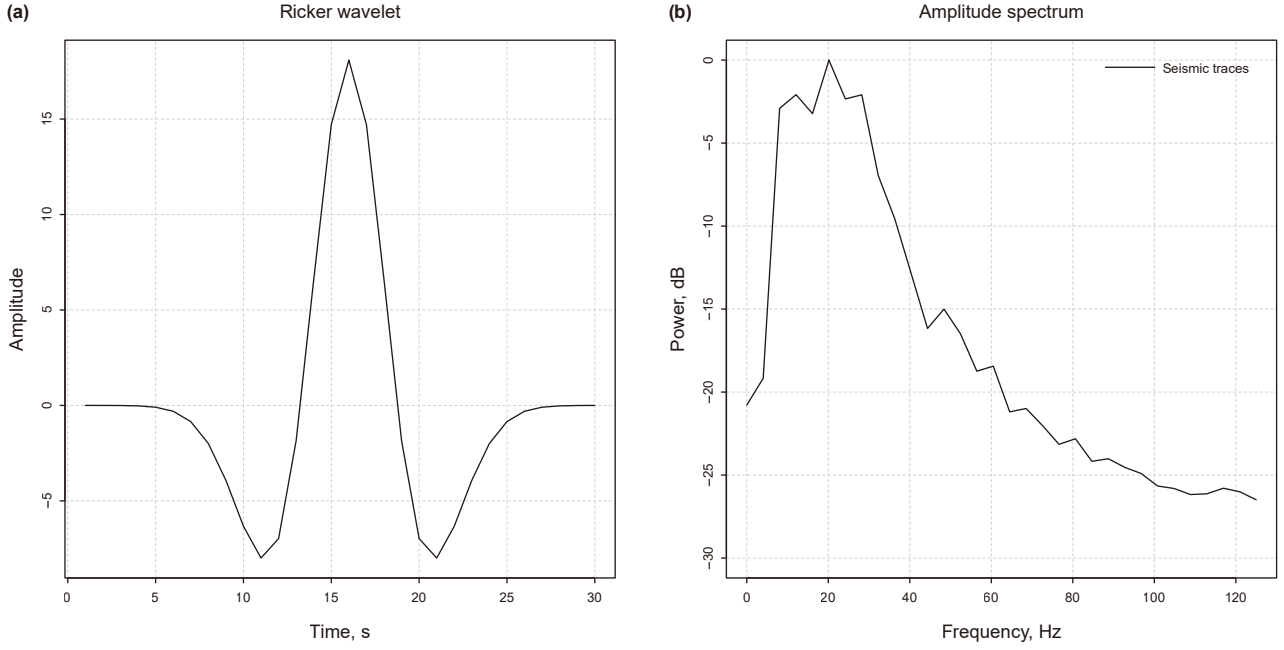

Fig. 3. Left: Ricker wavelet with a frequency of 20.16 Hz. Right: Amplitude spectrum calculated from the nearest inline seismic section.

4.3. Variographic analysis of petrophysical and seismic properties

Variogram models were estimated for the subsampled acoustic impedance and total porosity. Three models were tested: exponential, Gaussian, and spherical. The best-fit model for acoustic impedance was spherical, with a sill of 375,000, a range of 62 ms, and a nugget of 500 (Fig. 6(a)). For total porosity, the spherical model was also selected, with a sill of 0.0004, a range of 50 ms, and a nugget of zero (Fig. 6(b)).

Table 1
Basic statistics of (AI, ϕ_t) well logs at well scale, upscaled, and subsampled resolutions.

Statistics	AI	AI	AI	ϕ_t	ϕ_t	ϕ_t
		Upscaled	Subsampled		Upscaled	Subsampled
Samples	3696	3696	63	3696	3696	63
Minimum	5086.007	5835.096	5840.124	0.062	0.165	0.167
1st quartile	6157.005	6178.118	6159.766	0.214	0.212	0.215
Median	6809.557	6831.465	6450.822	0.229	0.231	0.232
Mean	6968.283	6892.898	6817.802	0.221	0.222	0.223
3rd quartile	7321.616	7353.490	7254.240	0.241	0.236	0.236
Maximum	11661.464	8891.212	8838.185	0.293	0.261	0.257
Range	6575.456	3056.115	2998.060	0.231	0.095	0.089
Interquartile range	1164.611	1175.372	1094.474	0.026	0.024	0.021
Variance	1310302.936	708798.264	687258.826	0.001	0.0005	0.0005
Standard deviation	1144.684	841.901	829.010	0.033	0.022	0.021
Skewness	1.561	0.596	0.684	−1.810	−1.213	−1.303
Kurtosis	5.765	2.189	2.350	6.996	3.241	3.722

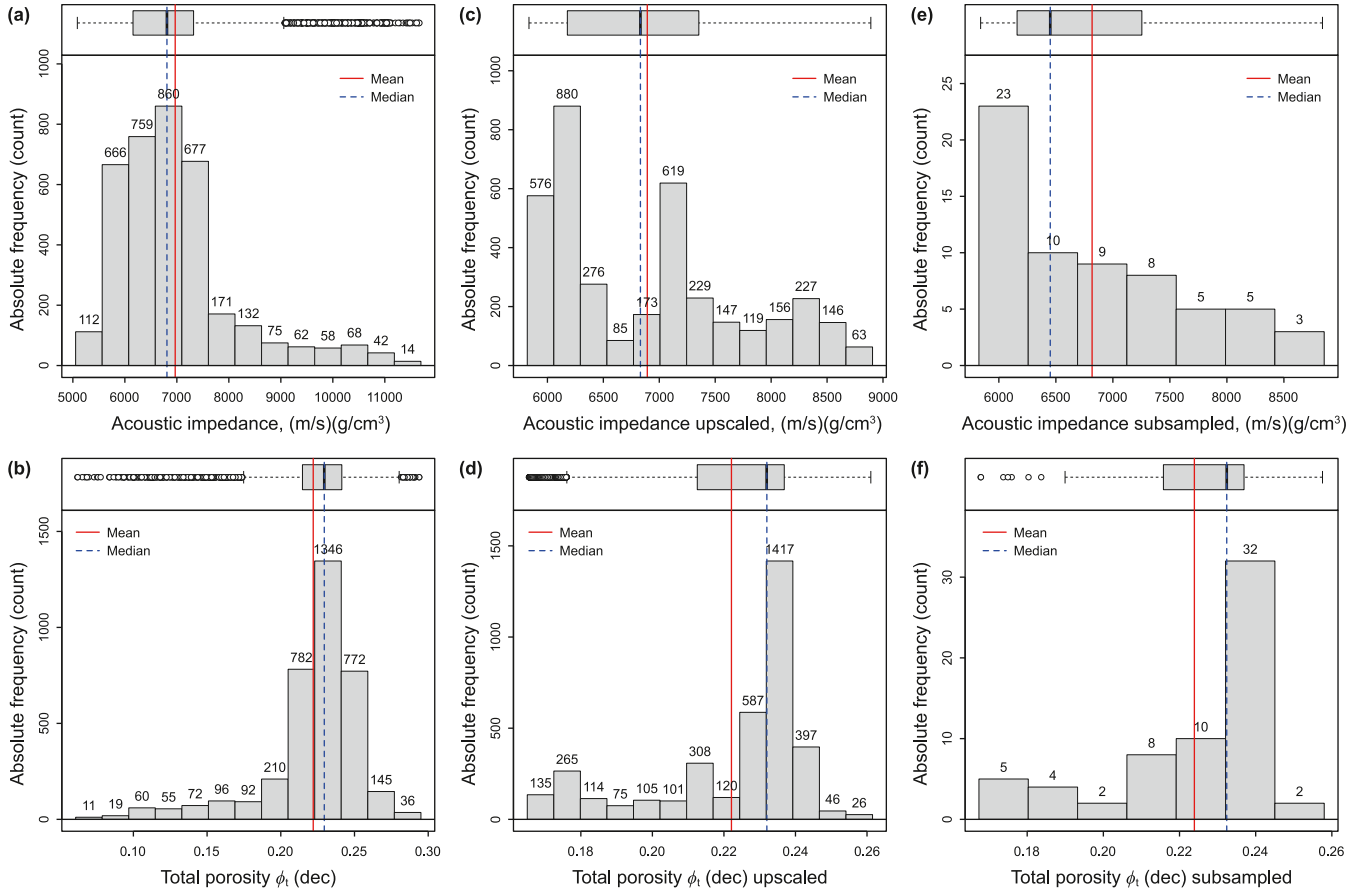

Fig. 4. Histograms of acoustic impedance AI **(a)**, total porosity ϕ_t **(b)**, upscaled AI **(c)**, upscaled ϕ_t **(d)**, subsampled AI **(e)**, and subsampled ϕ_t **(f)**.

5. Method validation: geostatistical seismic inversion based on copulas

5.1. Bayesian estimation of the dependence model

This section applies the Bayesian inference framework described in Section 3.3 to estimate the joint distribution model that characterizes the dependence between acoustic impedance and total porosity. The posterior parameters used in this section are obtained through the two-stage updating process, where well-log-based priors are first refined using upscaled logs and then validated with subsampled data. These posterior estimates form the core of the forward model used in the seismic inversion.

The results of the parametric analysis are presented in the work by Vázquez-Ramírez et al. (2023). That study demonstrated that the functions most compatible with geophysical well logs are, in order of suitability: the lognormal distribution is optimal for acoustic impedance, the Weibull distribution is optimal for total porosity, and the Frank copula model is optimal for the dependence structure. Thus, the prior model consists of five parameters: the lognormal parameters (log μ, log σ) and its normalized marginal u representing acoustic impedance; the Weibull parameters (α, λ) and its normalized marginal v representing total porosity;

Table 2
Dependence measures of (AI, ϕ_t) for well log, upscaled, and subsampled cases.

Dependence measure	Pearson	Spearman	Kendall
(AI, ϕ_t) well log	−0.8563	−0.7107	−0.5335
(AI, ϕ_t) upscaled	−0.9063	−0.8692	−0.7010
(AI, ϕ_t) subsampled	−0.9026	−0.8673	−0.6989

and the Frank copula dependence parameter (θ). The prior function is expressed as:

$$\mathbb{P}(\mathbf{m}) = \pi(\log \mu, \log \sigma, \alpha, \lambda, \theta) \tag{6}$$

The likelihood function is given by:

$$\mathbb{P}(\mathbf{d}|\mathbf{m}) = c_\alpha(u, v)\cdot f_1(x_1; \log \mu, \log \sigma)\cdot f_2(x_2; \alpha, \lambda) \tag{7}$$

where f_1 is the lognormal density function evaluated with acoustic impedance samples (x_1), f_2 is the Weibull density function evaluated with total porosity samples (x_2), and $c_\alpha(u, v)$ is the Frank copula density function (Eq. (A.10)). The posterior distribution $\mathbb{P}(\mathbf{m}|\mathbf{d})$ is obtained by combining Eqs. (6) and (7).

The Random Walk Metropolis-Hastings algorithm was used to estimate the posterior parameters. Normal distributions were assumed for all parameters, with means defined by their prior values and variances defined as a percentage of the prior value. The variance was chosen to ensure an acceptance rate between 20% and 30%. A total of 10,000 iterations were performed.

In the first iteration, the prior parameter values were initialized using the optimal fits to well-log samples based on the Akaike Information Criterion (AIC). These values are listed in Table 3, second column. The parameters were then updated using the upscaled geophysical well logs. To maintain the desired acceptance rate of 23.5%, only four of the five parameters were used in the update, as the initial θ parameter restricted convergence. As shown in Table 3, fourth column, the parameters of the lognormal and Weibull distributions exhibit minimal change. However, the comparison of prior and posterior cumulative distributions in Fig. 7(a) and (c) shows significant shifts. The posterior distribution is considered

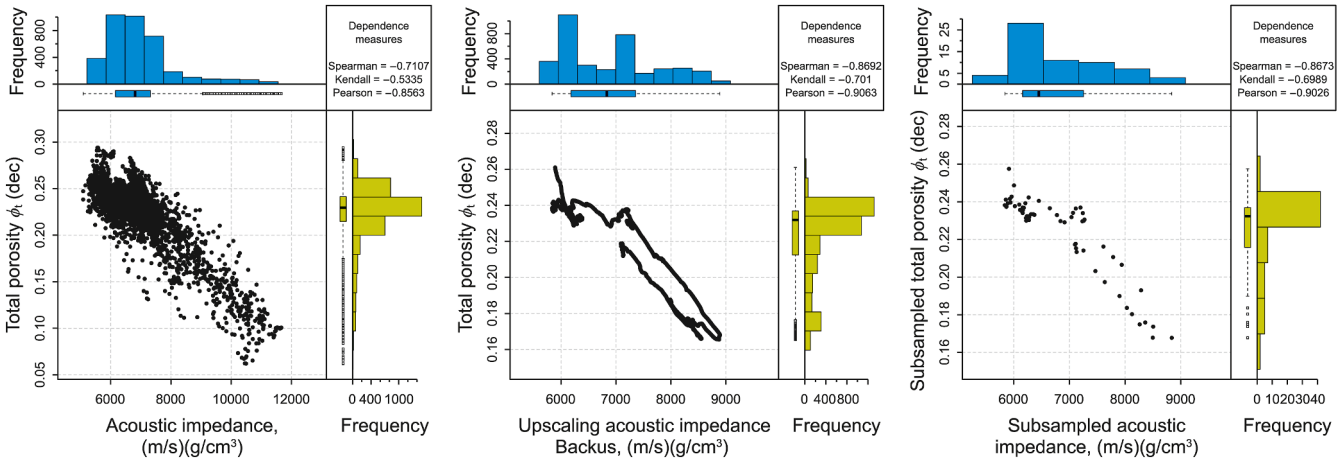

Fig. 5. Scatter plots of (AI, ϕ_t) well log (left), upscaled log (center), and subsampled log (right).

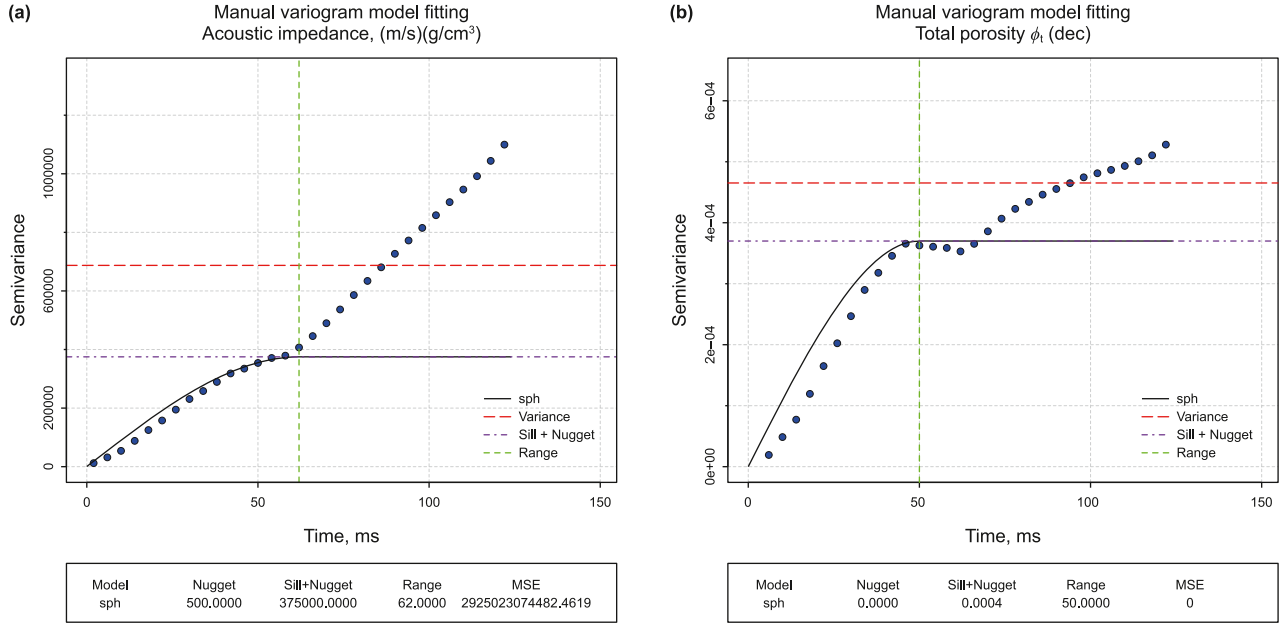

Fig. 6. **(a)** Variogram model of acoustic impedance. **(b)** Variogram model of total porosity. Both estimated in the time domain.

Table 3
Prior and posterior parameter values. First priors were estimated using well-scale samples; second priors are posteriors from upscaled logs. Final posterior values were estimated using subsampled logs.

Parameter	1st prior (well logs)	Variance, %	2nd prior (upscaled logs)	Variance, %	Posterior (subsampled logs)
Lognormal (μ)	8.837	1.800	8.804	1.700	8.790
Lognormal (σ)	0.150	1.800	0.151	1.700	0.151
Weibull (α)	9.373	1.800	9.400	1.700	9.330
Weibull (λ)	0.234	1.800	0.235	1.700	0.237
Frank copula (θ)	−6.265	–	−12.600	2.300	−21.000

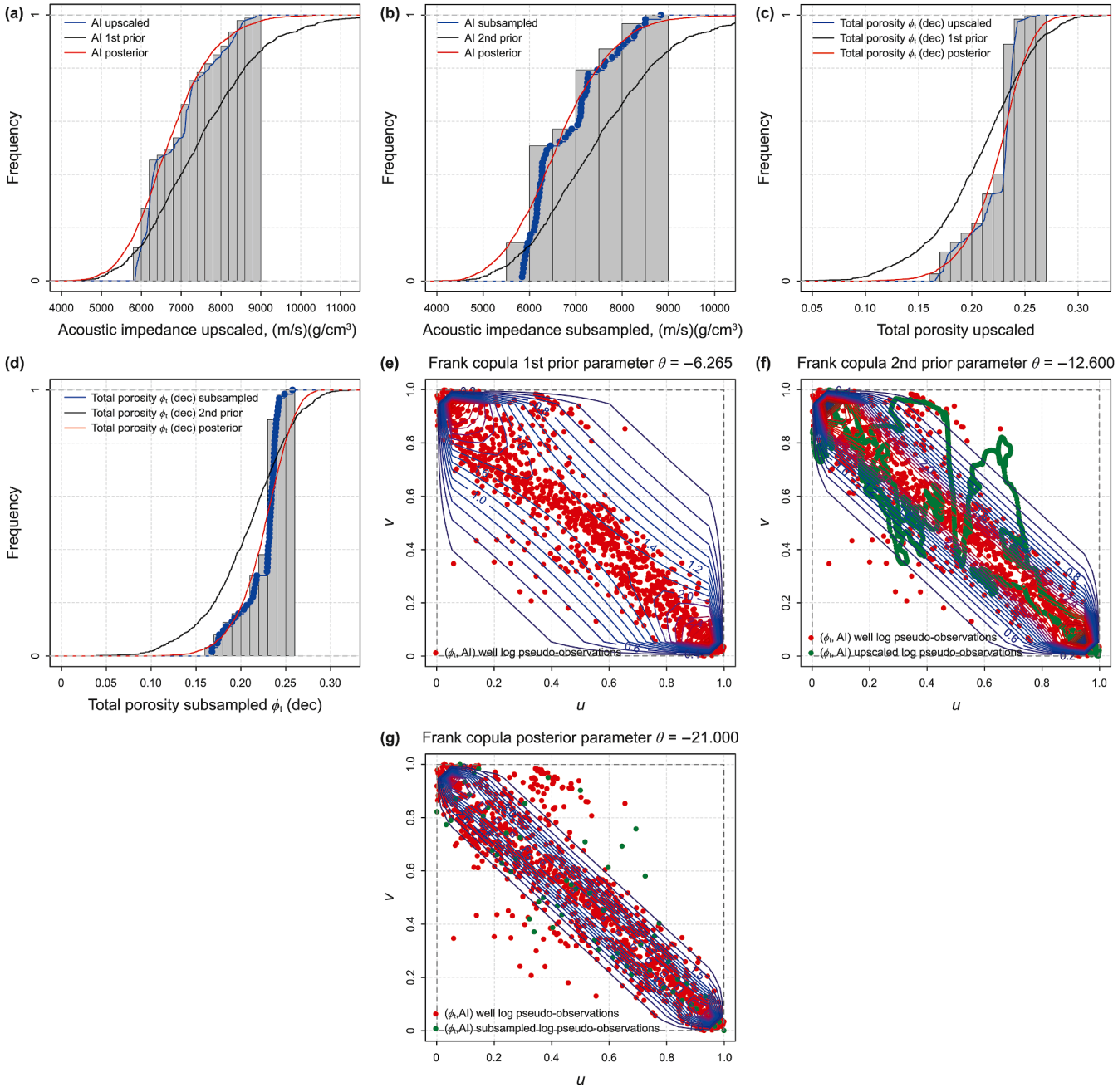

Fig. 7. **(a)** Posterior distribution of AI using upscaled logs, **(b)** posterior distribution of ϕ_t using upscaled logs, **(c)** posterior distribution of AI using subsampled logs, **(d)** posterior distribution of ϕ_t using subsampled logs, **(e)** prior dependence model, **(f)** posterior dependence model using upscaled logs, and **(g)** posterior dependence model using subsampled logs. The blue contour lines in panels (e), (f) and (g) represent iso-density levels of the fitted copula density function, illustrating the dependence structure between the pseudo-observations.

acceptable given its proximity to the empirical distribution of the upscaled logs. Although the posterior θ value increased to −12.6, this aligns with the increased dependence observed in Tables 2 and is also visible in Fig. 7(e) and (f), which show how the model captures the distribution of pseudo-observations.

In a second iteration, the posterior parameter values from the first search were used as priors, and the new information was the subsampled logs. This time, all five parameters were included, and the acceptance rate was 21.5%. As seen in Table 3, sixth column, most parameters changed only slightly—except for the dependence parameter θ, which shifted from −12.6 to −21. While this is a substantial change, it reflects the increase in dependence documented in Table 2. It is worth noting that the Frank copula parameter can range between −100 and 100 (Joe, 2014).

5.2. Seismic inversion using the nearest borehole trace

The objective of geostatistical seismic inversion is to solve the inverse problem by simulating elastic properties that reproduce the observed seismic trace under a given forward model. In this study, the convolutional model is used, requiring two components: a wavelet and a reflectivity series. The wavelet is the 20.16 Hz Ricker wavelet, and the reflectivity series is computed from acoustic impedance as described in Section 4.1. Multiple realizations of acoustic impedance are generated to minimize the squared error between synthetic and observed seismic traces. The seismic trace closest to the well, located at 18.5 m, is used for validation.

Simulated annealing is used to generate realizations of acoustic impedance and total porosity. The initial image is the subsampled log data, and the search function employs the dependence model from Section 5.1. The objective functions are the variogram model of Fig. 6(a) and the RMS between the synthetic and real seismic traces. Once the best-fitting acoustic impedance realization is found, it is used as a conditional variable to simulate total porosity using the same dependence model. The variogram model for porosity (Fig. 6(b)) is used as the objective function. For all simulations, simulated annealing is initialized with a temperature of 0.001, a cooling parameter of 0.22, and stops at a convergence value of 0.0001 or after 20,000 iterations.

As shown in Table 4, the statistics for acoustic impedance and porosity are consistent across well, subsampled, and simulated data. However, differences between the seismic and synthetic traces are notable in minimum, maximum, and first quartile, exceeding 1000 units. Visually, the seismic and synthetic traces in Fig. 8(a) are closely aligned, with only minor discrepancies. Similarly, the acoustic impedance and porosity simulated from the dependence model closely resemble the subsampled logs (Fig. 8(b) and (c)). These results indicate that the copula-based inversion method is effective.

6. Application case using seismic inline section

Using the results from the seismic trace nearest to the well, a trace-by-trace scheme was employed to simulate acoustic impedance across a seismic inline section. The dimensions of this inline section are as follows: the *Y*-axis spans 248 m, and the *X*-axis spans 612 m. These dimensions are divided into 32 traces, with a spacing of 4 m along the *Y*-axis. The results of this application are presented below.

As shown in Fig. 10, the amplitude spectrum of the synthetic traces estimated via the simulated annealing method closely approximates that of the original seismic image in the frequency range between 0 and 50 Hz. Moreover, both spectra exhibit a similar dominant frequency, confirming the consistency of the synthetic response with the real data.

In Fig. 9(a), the original seismic inline is shown, while Fig. 9(b) displays the inline constructed from the synthetic traces estimated using simulated annealing. The similarity between the two images is evident, with a calculated error ranging from 2% to 10%, as illustrated in Fig. 9(c). Areas of higher standard deviation, particularly between 20,980–20,990 and 3300–3350, may correspond to zones of high seismic amplitude and could be attributed to abrupt changes in facies.

Fig. 9(d) shows the acoustic impedance section obtained from the synthetic traces. The structures derived from the simulated annealing method align well with the well log. For example, the high acoustic impedance zone between 3300 and 3350 ms corresponds to a similar zone in the well log. Another structure between 3200 and 3250 ms exhibits positive amplitude, suggesting a small high-impedance body not observed in the well log. This may be due to the well not intersecting the structure directly, although its proximity allowed it to be detected by the seismic survey.

Furthermore, a total porosity prediction was made using the dependence model, with acoustic impedance from each trace serving as the conditioning variable. The resulting porosity image, simulated from the acoustic impedance via the simulated annealing method and shown in Fig. 9(e), displays a high degree of consistency with the upscaled well log. A zone of low porosity is observed between 3300 and 3350 ms. In contrast, the structure between 3200 and 3250 ms does not appear to exhibit a significantly different porosity, suggesting that its porosity is comparable to that of adjacent intervals.

The anomaly between 3300 and 3350 ms, characterized by high acoustic impedance and low porosity, is consistent with a more

Table 4
Descriptive statistics of the seismic and synthetic traces, acoustic impedance, and total porosity from subsampled and simulated data.

Statistics	Seismic	Synthetic	AI subsampled	AI simulated	ϕ_t subsampled	ϕ_t simulated
Samples	63	63	63	63	63	63
Minimum	−26641.828	−24934.981	5840.124	5842.385	0.167	0.170
1st quartile	−3642.293	−3465.436	6159.766	6220.179	0.215	0.217
Median	2596.174	1946.605	6450.822	6652.424	0.232	0.226
Mean	258.079	176.649	6817.802	6676.113	0.223	0.224
3rd quartile	5913.707	6287.291	7254.240	6806.351	0.236	0.237
Maximum	15073.054	13508.371	8838.185	8194.131	0.257	0.255
Range	41714.882	38443.352	2998.060	2351.746	0.089	0.085
Interquartile range	9556.000	9752.728	1094.474	586.171	0.021	0.019
Variance	85621835.670	76456030.042	687258.826	334984.199	0.0005	0.0003
Standard seviation	9253.206	8743.913	829.010	578.778	0.021	0.018
Skewness	−1.145	−0.891	0.684	0.982	−1.303	−0.754
Kurtosis	3.821	0.616	−0.602	0.632	3.722	0.713

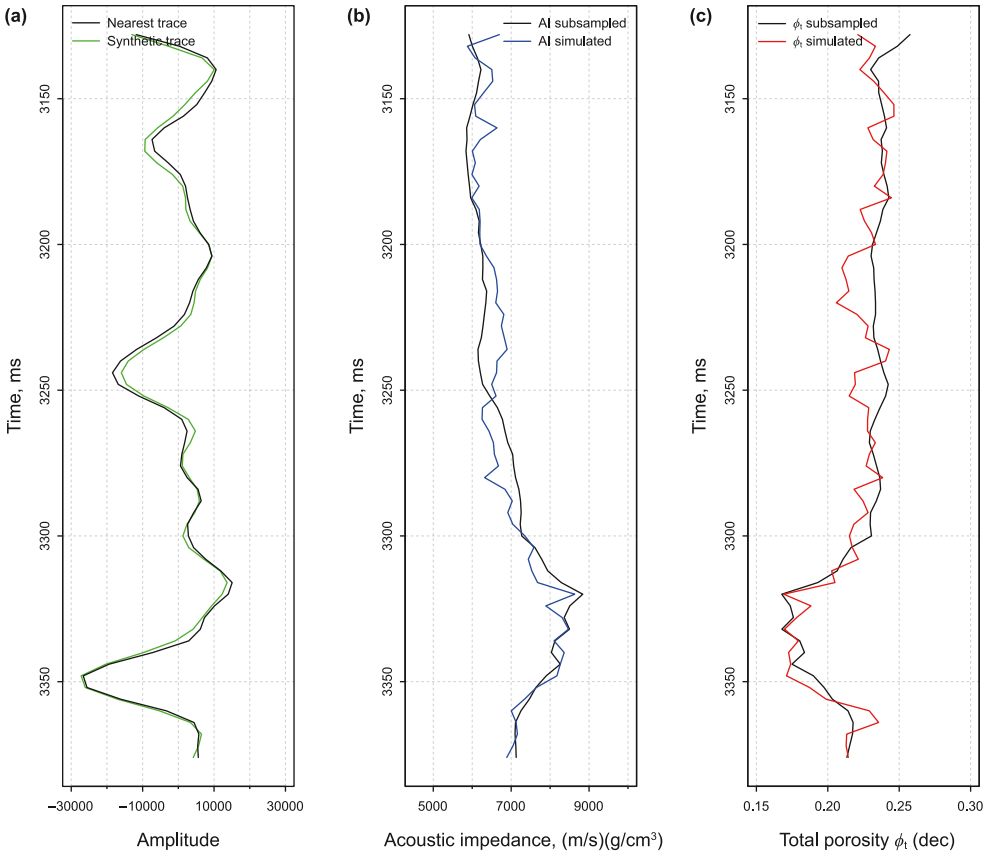

Fig. 8. **(a)** Seismic vs. synthetic trace with lowest quadratic error. **(b)** Subsampled vs. simulated acoustic impedance. **(c)** Subsampled vs. simulated total porosity (conditioned to acoustic impedance).

compacted or lithologically distinct interval, possibly indicative of a tighter sandstone or reduced reservoir quality. This interpretation is supported by well-log data and aligns with the seismic response observed in the original inline section.

Given the strong match between the synthetic and observed seismic traces, and the agreement with log-based petrophysical trends, we interpret this anomaly as a genuine geological feature rather than an artifact or noise. As such, its presence enhances rather than detracts from the reliability of the inversion results by confirming the method's ability to resolve laterally continuous, high-contrast features consistent with ground truth.

7. Discussion

As shown in Section 5.1, the Bayesian approach yielded a posterior dependence model that is consistent with the well-log information. While the marginal distributions remained relatively stable despite upscaling and subsampling, the dependence parameter θ experienced a significant change—from -6.265 to -21. Interestingly, the Spearman dependence measure did not exhibit a corresponding large change, highlighting the sensitivity of the copula parameter to the joint structure.

When comparing the cumulative distribution function (CDF) generated using the posterior parameter values against total porosity ϕ_t, Fig. 7(c) shows good agreement with the scaled porosity values, particularly in the range of 0.17–0.23. At higher porosity values, however, some deviation is observed. For acoustic impedance (Ip), Fig. 7(a) reveals that the posterior cumulative distribution closely follows the scaled CDF, with only minor discrepancies between 5950 and 6200 (m/s)·(g/cm^3). The posterior fits shown in Fig. 7(c) and (d) represent improvements over the scaled distributions.

The acoustic impedance results obtained via the simulated annealing method also demonstrate high consistency with the subsampled logs. As shown in Table 4, most statistical descriptors are comparable between the simulated and subsampled acoustic impedance, with the main exception being variance. Similarly, the total porosity simulation yields statistics that closely match those of the subsampled data.

Another notable observation is the use of subsampled logs as the initial image in the simulation process. This contributes to consistency with the borehole structure and facilitates alignment with seismic features. For instance, the degradation pattern in the amplitude value between 20,963 and 20,970 reveals a decrease in acoustic impedance that corresponds to a polarity reversal in the seismic trace—from positive to negative—highlighting the inversion method's sensitivity to seismic features.

The current implementation assumes uniform vertical resolution across the seismic inline, and the well-log data were upscaled accordingly. Total porosity was averaged using a moving window equivalent to the vertical seismic resolution, and acoustic impedance was computed using the Backus averaging method applied to V_p and ρ logs. The dominant frequency of the seismic signal, estimated at 20.16 Hz (see Fig. 3), was used to define the resolution scale. While this approach mitigates resolution mismatch, seismic data often exhibit variable resolution due to acquisition and processing differences. Future work will incorporate adaptive upscaling strategies or multiresolution inversion frameworks (Bunks et al., 2012), enabling the model to better adapt to spatially variable resolution and improve inversion accuracy.

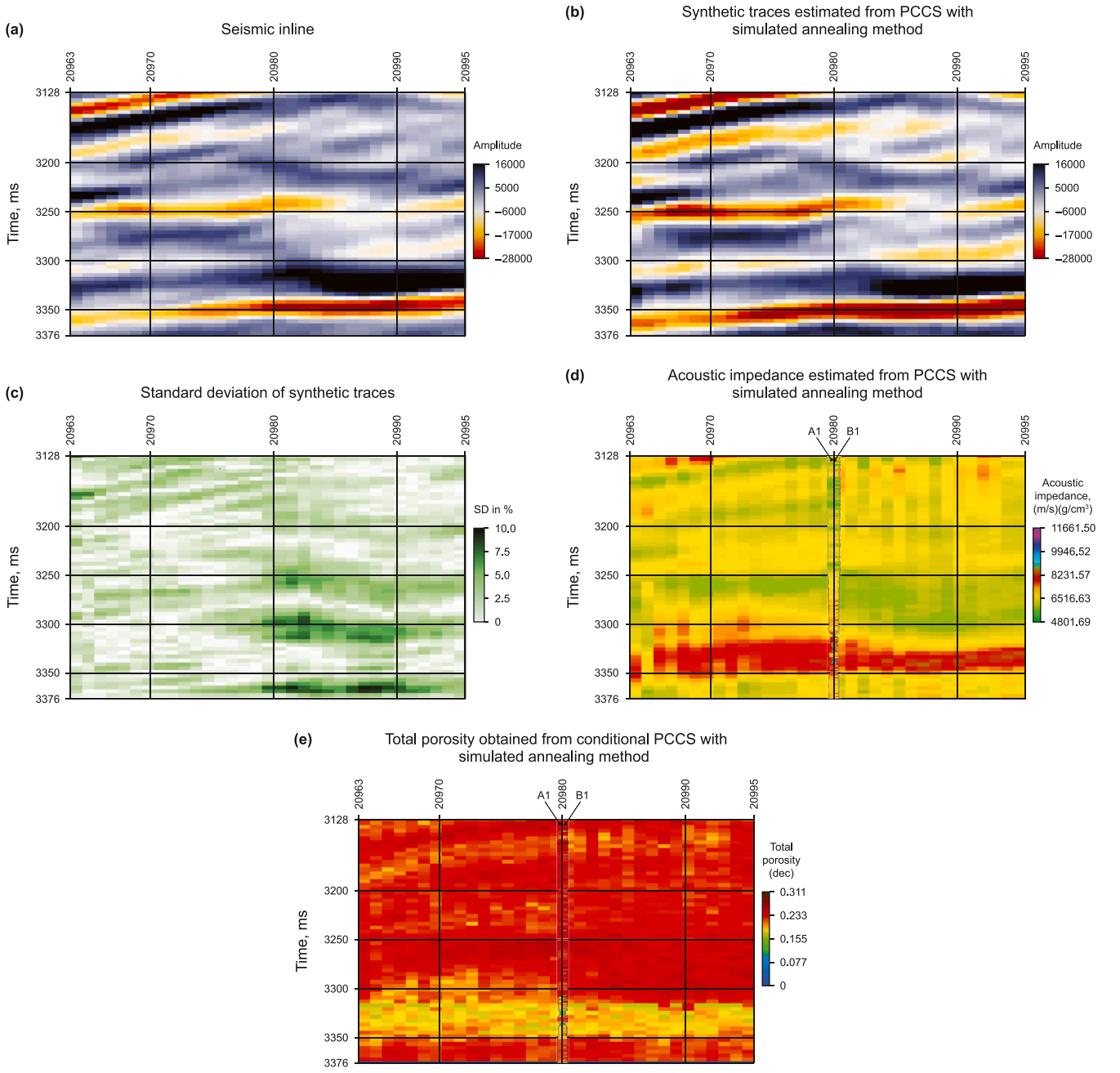

Fig. 9. (**a**) Seismic image. (**b**) Synthetic traces estimated using the simulated annealing method. (**c**) Standard deviation of the synthetic traces. (**d**) Acoustic impedance derived from the synthetic traces. (**e**) Total porosity predicted using simulated annealing. A1 is the upscaled well log; B1 is the original geophysical well log.

A key limitation of the current implementation is the absence of lateral variogram modeling. The inversion was carried out using a trace-by-trace scheme with vertical variograms estimated in the time domain, restricting spatial continuity to the vertical direction. Although the inverted sections display structural coherence that aligns with the well data and reflectivity patterns, the lack of lateral spatial constraints may limit the model's ability to capture horizontally extensive geological features. Future efforts will focus on integrating three-dimensional spatial models by including lateral variograms derived from seismic attributes or well-log correlations, thereby improving the realism and consistency of the simulated volumes.

While the proposed method demonstrates stable and consistent results using parametric copulas, it is important to acknowledge the trade-offs associated with this choice. Parametric copulas, such as the Frank copula used here, are less flexible than non-parametric alternatives like Bernstein copulas. Their analytical structure imposes assumptions that may limit accuracy in datasets with tail asymmetry or multimodal joint behavior. Nonetheless, parametric copulas offer computational efficiency, interpretability, and ease of integration into a Bayesian framework, making them suitable for moderately complex dependencies like the negatively correlated acoustic impedance and porosity in this study. Users are advised to evaluate the dependence structure in their data before selecting a copula model. Future work may explore hybrid approaches that combine the efficiency of parametric forms with the flexibility of non-parametric models to handle more complex geological scenarios.

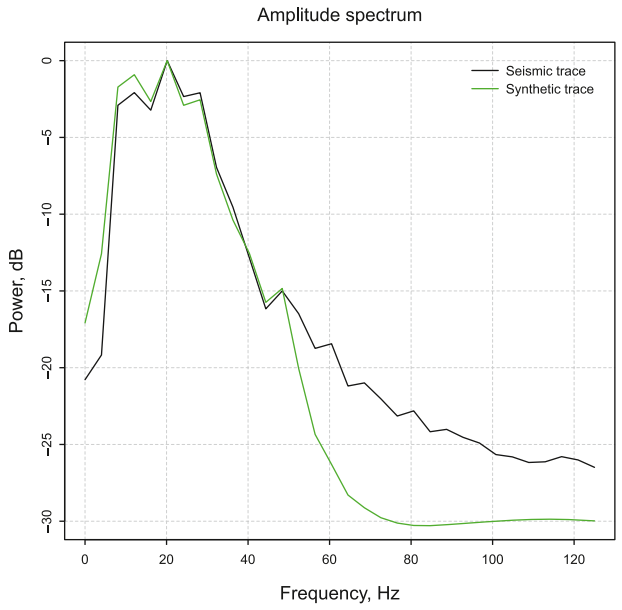

Fig. 10. Comparison of amplitude spectra between the original seismic image and the image with synthetic traces.

Scalability to large-scale datasets is another consideration. Although parametric copulas reduce the computational cost, the current inversion framework is constrained by the trace-by-trace simulation scheme and reliance on MCMC for Bayesian estimation. As such, the method is best suited for 2D lines or small-to-moderate 3D volumes. To improve scalability, future developments will explore parallelized simulations across traces, as well as more efficient inference techniques (e.g., variational Bayes, Hamiltonian Monte Carlo). Global optimization strategies may also reduce dependence on repeated forward modeling, enabling the method's application to high-resolution 3D seismic datasets.

Another limitation of this study is the use of a single well to define marginal distributions and dependence structure. This choice was driven by data availability: while neighboring wells exist, most lack total porosity or acoustic impedance logs. Nevertheless, multi-well integration would increase the statistical robustness and spatial representativeness of the joint model. In future applications, this could be achieved by jointly estimating copula parameters across multiple wells or allowing spatially varying copula models. Additional wells would also improve variogram calibration and simulation conditioning, especially in areas far from the reference well.

A broader methodological perspective is also valuable to assess how the proposed approach compares with existing geostatistical seismic inversion (GSI) techniques. Table 5 presents a qualitative comparison across several criteria, including inversion targets, simulation techniques, optimization strategies, noise robustness, uncertainty quantification, and key strengths and limitations. This synthesis helps situate our copula-based inversion method among traditional approaches such as sequential Gaussian simulation (SGS), direct sequential simulation (DSS), and AVA/AVO elastic inversion.

This comparative overview emphasizes that the proposed copula-based approach offers a balanced trade-off between modeling flexibility and computational efficiency. In particular, it is well suited for scenarios involving nonlinear dependence or weak correlation between petrophysical and elastic attributes—conditions under which traditional Gaussian-based methods may underperform. Although the current implementation lacks lateral continuity modeling and is optimized for small-to-moderate scale applications, its conceptual framework is extensible to more complex and higher-dimensional problems.

8. Conclusions

The joint seismic inversion of elastic and petrophysical properties using copula-based stochastic co-simulation models presents a novel approach that enables the simultaneous simulation of both property types using a flexible dependence structure, without assuming a predefined joint probability distribution. The method is effective for generating spatially consistent realizations, particularly when the principal elastic attribute (acoustic impedance) is used as a conditioning variable. Furthermore, new data from additional wells or seismic surveys can be integrated into the model via a Bayesian inference framework.

By embedding the copula-based dependence model into the forward modeling process, the Bayesian approach enables the estimation of posterior parameters using both scaled and subsampled log samples. The resulting joint posterior distribution supports robust simulations through simulated annealing, yielding stable elastic and petrophysical models that honor both geophysical and statistical constraints.

The inversion results demonstrate that, when acoustic impedance is available at the seismic scale, the copula-based method can generate predictive realizations of petrophysical properties—such as total porosity—that are consistent with upscaled well-log data. These realizations preserve key spectral characteristics, including

Table 5
Comparison of geostatistical seismic inversion methodologies.

Criteria	Trace-by-trace GSI	Global GSI (DSS)	Global elastic inversion	Seismic AVA/AVO inversion	Copula-based joint GSI
Inversion target	Local elastic attribute	Global elastic attribute	Global elastic attribute	ρ, V_p, V_s (pre-stack)	Elastic and petrophysical attribute
Simulation technique	SGS	DSS	DSS and co-DSS	DSS and co-DSS	PCCS
Optimization approach	Monte Carlo algorithm	Genetic Algorithm	Genetic Algorithm	Weighted genetic algorithm	Simulated annealing
Noise handling	Poor in low SNR	Robust	High robustness	Very robust	High
Uncertainty quantification	High	High	High	Very high	High
Strengths	Simple; fast; good with clean data	Captures spatial continuity	Multi-property elastic modeling	Full elastic recovery	Flexible for nonlinear dependence
Limitations	Sensitive to noise; lacks global consistency	Requiring significant computational resources	Requires high-quality logs	Pre-stack data requirement; high cost	Trace-by-trace may lack lateral continuity; best for 2D/small 3D

the dominant frequency and bandwidth of the seismic signal, and align well with observed reflectivity patterns.

While the method currently employs vertical variograms and a trace-by-trace inversion scheme, it produced coherent spatial distributions in both acoustic impedance and porosity. Future research will incorporate lateral variogram modeling to enhance horizontal continuity and structural realism.

The use of parametric copulas, particularly the Frank copula, provides a balance between modeling capacity and computational efficiency. Although less flexible than non-parametric alternatives, parametric copulas are well-suited for moderate complexity datasets, such as the negatively correlated acoustic impedance and porosity observed in this case study.

This framework is most applicable to 2D seismic lines or small-to-moderate 3D volumes. Future extensions will focus on improving scalability through parallelized inversion routines and more efficient Bayesian inference techniques. Additionally, incorporating data from multiple wells and extending the framework to simulate multiple elastic and petrophysical properties such as those required in amplitude versus offset (AVO) inversion are promising directions for continued development.

CRediT authorship contribution statement

Daniel Vázquez-Ramírez: Writing – original draft, Software, Project administration, Methodology, Investigation, Formal analysis. **Martín A. Díaz-Viera:** Writing – review & editing, Validation, Supervision, Resources, Formal analysis, Conceptualization. **Raúl del Valle-García:** Writing – review & editing, Visualization, Supervision, Formal analysis.

Supplementary material

A PDF version of the code and accompanying notes, developed using Jupyter notebooks in R, is available at the following GitHub repository: https://github.com/esmg-mx/Copula-Base-modelling.

The computational implementation was carried out in the R programming language. The statistical analysis and joint inversion method used the following libraries: copula (Hofert et al., 2019), fitdistrplus, LearnBayes (Albert, 2009), RSEIS, NMOF, and RGEOSTAD (Díaz-Viera et al., 2021).

Declaration of competing interests

The authors declare the following financial interests/personal relationships which may be considered as potential competing interests: Daniel Vázquez-Ramírez reports financial support was provided by National Autonomous University of Mexico. Daniel Vázquez-Ramírez reports a relationship with National Autonomous University of Mexico that includes: employment. If there are other authors, they declare that they have no known competing financial interests or personal relationships that could have appeared to influence the work reported in this paper.

Acknowledgments

The data were provided by the National Hydrocarbons Commission of Mexico, according to appendix C of the license to use the information in favor of Universidad Nacional Autónoma de México, dated December 11, 2017, under the nomenclature CNIH-C-00417.305. This reference information is the property of Mexico and its collection, safekeeping, use, administration and updating, as well as its publication is only authorized to the National Hydrocarbons Commission. Data will be shared on request to the corresponding author with permission of the National Hydrocarbons Commission.

Appendix A. Parametric Archimedean copula models

Appendix A.1. Copula definition

As defined by (Nelsen, 2006), a copula is *"a function that joins or couples multivariate distribution functions to their one-dimensional marginal distribution functions"*. If you want to use copulas in the field of statistics, you should use Sklar's theorem. Sklar's theorem is defined as: Let H be a joint distribution function with margins F and G. Then there exists a copula C such that for all (x, y) in $\overline{R}$.

$$H(x,y) = C(F(x), G(y)) \tag{A.1}$$

If $u = F(x)$ and $v = G(y)$ are marginal distribution functions and $C(u, v) = C(F(x), G(y))$ is a valid distribution function, then for any copula $C(u, v)$ its partial derivatives are $\frac{\partial C}{\partial u}$ and $\frac{\partial C}{\partial v}$ exist for almost all (u, v) in [0; 1]. Then $\frac{\partial C}{\partial u \partial v}$ and $\frac{\partial C}{\partial v \partial u}$ exist and are continuous on I^2. If this is true, the density function of the copula is

$$c(u,v) = \frac{\partial^2(C)}{\partial u \partial v} \tag{A.2}$$

And the joint probability density function of x and y is given by

$$f(x,y) = \frac{\partial^2(C)}{\partial u \partial v} \cdot \frac{\mathrm{d}F}{\mathrm{d}x} \cdot \frac{\mathrm{d}G}{\mathrm{d}y} \tag{A.3}$$

Appendix A.2. Definition of Archimedean copulas

Parametric copulas represent a specific type of copulas, offering the advantage of controlling the dependence between variables through the use of parameters associated with the joint distribution function. This approach is applicable across three primary families of parametric copulas, namely elliptic, extreme value, and Archimedean (Joe, 2014). In this work, we will limit our discussion to the Archimedean copula.

In strict technical terms, Eq. (A.4) is the Archimedean equation.

$$C(u,v) = \varphi^{[-1]}(\varphi(u) + \varphi(v)) \tag{A.4}$$

where the function φ is called *copula generator*. If $\varphi(0) = \infty$, φ is strictly generator, then $\varphi^{[-1]} = \varphi^{-1}$ and $C(u, v) = \varphi^{[-1]}(\varphi(u) + \varphi(v))$ and is said to be strictly an Archimedean copula.

Let *varphi* be a strictly decreasing continuous function of $\mathbf{I}$ on the interval $[0, \infty]$ such that $varphi(1) = 0$, the pseudo-inverse of φ is the function $\varphi^{[-1]}$ with $Dom\varphi^{[-1]} = [0, \infty]$ and $Ran\varphi^{[-1]} = \mathbf{I}$ given by

$$\varphi^{[-1]}(t) = \begin{cases} \varphi^{[-1]}(t), & \text{if} \quad 0 \le t \le \varphi(0) \\ 0, & \text{if} \quad \varphi(0) \le t \le \infty \end{cases} \tag{A.5}$$

Another significant attribute is the Archimedean density copula, which can be derived from the generator and its derivatives as follows (Shemyakin and Kniazev, 2017):

$$c(u,v) = \frac{\partial^2 C(u,v)}{\partial u \partial v} = -\frac{\varphi''(C(u,v))\varphi'(u)\varphi'(v)}{(\varphi'(C(u,v)))^3} \tag{A.6}$$

Appendix A.3. Frank copula

This family of copulas is very popular because it can be used in models with positive and negative dependencies. It is a symmetric copula in both tails and includes both Frechet bounds in the entire $(-infty, \infty)$ region. The disadvantage of the Frank copula is that the dependence tends to be weak in the tails and

strong in the central part, as can be seen in the density function of Fig. A.1. Therefore, it is recommended to use this type of copula when the dependence model has tails with low dependence (Trivedi and Zimmer, 2007).

Frank copula is defined as (Shemyakin and Kniazev, 2017)

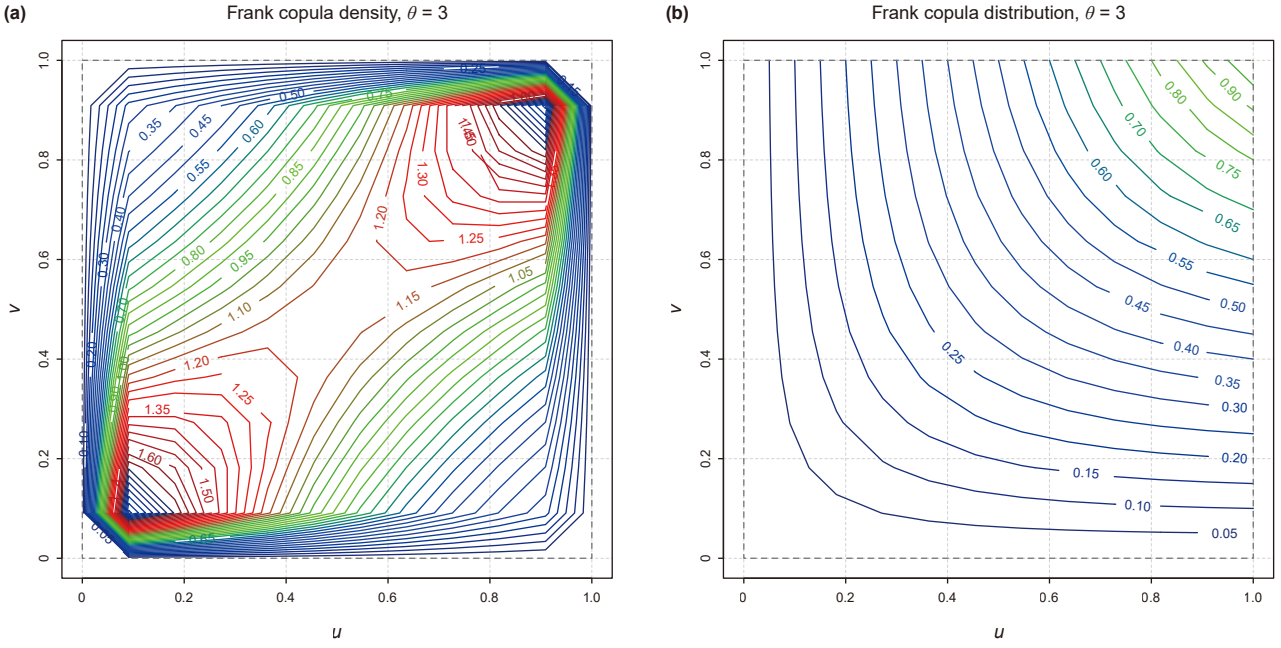

Fig. A.1. Projection on the *u*-*v* plane of: **(a)** the density function and **(b)** the probability function of a bivariate Frank copula (red regions indicate a higher degree of dependence).

$$C_\alpha(u,v) = -\frac{1}{\alpha}\ln\left(1+\frac{(e^{-\alpha u}-1)(e^{-\alpha v}-1)}{(e^{-\alpha}-1)}\right), \qquad \alpha \neq 0 \tag{A.7}$$

Its generator is

$$\varphi(t) = -\ln\frac{e^{-\alpha t}-1}{e^{-\alpha}-1} \tag{A.8}$$

Its pseudo-inverse is

$$\varphi^{[-1]}(s) = -\frac{1}{\alpha}\ln[1+e^{-s}(e^{-\alpha}-1)] \tag{A.9}$$

The copula density function is

$$c_\alpha(u,v) = \frac{\alpha(1-e^{-\alpha})e^{-\alpha(u+v)}}{(e^{-\alpha}-1+(e^{-\alpha u}-1)(e^{-\alpha v}-1))^2} \tag{A.10}$$

Appendix B. Bayesian estimation of the joint distribution model

Bayesian inference provides a flexible framework for estimating the parameters of a joint distribution model based on copulas. This approach enables the integration of prior knowledge with observed data and supports the modeling of complex multivariate dependence structures. The framework is applicable to a wide range of problems where flexible joint distribution modeling is required, particularly in the presence of nonlinear or non-Gaussian dependence.

Appendix B.1. Prior information

In the Bayesian setting, prior distributions are assigned to the parameters of the marginal distributions and the copula. For each marginal variable X_i, the parameter α_i governs the shape of the univariate probability density function $f_i(x_i;\ \alpha_i)$. The dependence structure between variables is modeled using a copula density function $c(u_1, \ldots, u_d;\ \theta)$, where θ is the copula parameter and $u_i = F_i(x_i;\ \alpha_i)$ are the transformed uniform margins.

The prior distributions $\pi(\alpha_i)$ and $\pi(\theta)$ are typically selected empirically by fitting candidate parametric models to available data and evaluating them using statistical criteria such as the log-likelihood, Akaike Information Criterion (AIC; Hofert et al., 2019), and Bayesian Information Criterion (BIC; Claeskens and Hjort, 2008). Visual inspection using histograms and cumulative distribution functions may also be used to support model selection.

The joint prior distribution is defined as:

$$\pi(\theta,\alpha_1,\ldots,\alpha_d) = \pi(\theta)\prod_{i=1}^{d}\pi(\alpha_i), \tag{B.1}$$

where d is the number of variables.

Appendix B.2. Likelihood function

According to Bayes' theorem, given a sample of n observations $\mathbf{x}^{(j)} = (x_1^{(j)}, \ldots, x_d^{(j)})$, and assuming parametric marginal distributions $f_i(x_i;\ \alpha_i)$ and a copula density function $c(u_1, \ldots, u_d;\ \theta)$, the likelihood function is given by (Hofert et al., 2019):

$$\mathcal{L}(\mathbf{x}|\theta,\alpha_1,\ldots,\alpha_d)=\prod_{j=1}^{n} c\left(F_1(x_1^{(j)};\alpha_1),\ldots,F_d(x_d^{(j)};\alpha_d);\theta\right)\cdot\prod_{i=1}^{d} f_i(x_i^{(j)};\alpha_i), \tag{B.2}$$

where $u_i^{(j)}=F_i(x_i^{(j)};\alpha_i)$ are the univariate margins.

To improve numerical stability and computational efficiency, particularly in algorithms such as Metropolis-Hastings, the log-likelihood corresponding to Eq. (B.2) is used:

$$\log\mathcal{L}=\sum_{j=1}^{n}\log\left(c\left(F_1(x_1^{(j)};\alpha_1),\ldots,F_d(x_d^{(j)};\alpha_d);\theta\right)\right)+\sum_{i=1}^{d}\times\sum_{j=1}^{n}\log f_i(x_i^{(j)};\alpha_i). \tag{B.3}$$

Appendix B.3. Posterior model.

The posterior distribution is derived by combining the prior distribution (Eq. (B.1)) with the likelihood function (Eq. (B.2)). For a sample of n observations $\mathbf{x}$, the joint log-posterior is:

$$\begin{aligned}\log(\pi(\theta,\alpha_1,\ldots,\alpha_d|\mathbf{x}))\propto&\log(\pi(\theta))+\sum_{i=1}^{d}\log(\pi(\alpha_i))\\&+\sum_{j=1}^{n}\log\left(c\left(F_1\left(x_1^{(j)};\alpha_1\right),\ldots,F_d\left(x_d^{(j)};\alpha_d\right);\theta\right)\right)\\&+\sum_{i=1}^{d}\sum_{j=1}^{n}\log f_i\left(x_i^{(j)};\alpha_i\right),\end{aligned} \tag{B.4}$$

where $f_i(x_i;\ \alpha_i)$ are the marginal density functions and $c(\cdot)$ is the copula density function. The terms $x_i^{(j)}$ denote the observed values of variable X_i in sample j, and $F_i(x_i;\ \alpha_i)$ are the corresponding marginal cumulative distribution functions.

The posterior distribution captures the joint uncertainty in both the marginal parameters and the dependence structure. The estimation of these parameters is carried out using the Random Walk Metropolis-Hastings algorithm, as described in Section 5.1.

Appendix C. Backus averaging method

The Backus averaging method (Backus, 1962) is used to model the long-wavelength behavior of seismic waves propagating through a stack of thin, isotropic, horizontally layered media. Each layer is assumed to be isotropic and transversely homogeneous, and the averaging produces an equivalent transversely isotropic (TI) medium that captures the effective elastic behavior in the vertical direction.

Following Liner (2014), the method begins with well-log measurements of V_P, V_S, and density ρ, typically sampled at fine vertical resolution. These values define isotropic elastic layers via Hooke's law, where Lamé parameters λ and μ are computed as:

$$\begin{aligned}\mu&=\rho V_S^2,\\\lambda&=\rho\left(V_P^2-2V_S^2\right),\\\lambda+2\mu&=\rho V_P^2.\end{aligned} \tag{C.1}$$

From these, the stiffness coefficients (a, c, f, l, m) are determined for each layer. The Backus average then produces effective elastic coefficients (A, C, F, L, M) over a vertical window L_B:

$$\begin{aligned}A&=4\langle\frac{\mu(\lambda+\mu)}{\lambda+2\mu}\rangle+\langle\frac{1}{\lambda+2\mu}\rangle^{-1}\langle\frac{\lambda}{\lambda+2\mu}\rangle^{2},\\C&=\langle\frac{1}{\lambda+2\mu}\rangle^{-1},\\F&=\langle\frac{1}{\lambda+2\mu}\rangle^{-1}\langle\frac{1}{\lambda+2\mu}\rangle,\\L&=\langle\frac{1}{\mu}\rangle^{-1},\\M&=\langle\mu\rangle.\end{aligned} \tag{C.2}$$

The resulting effective stiffness parameters allow the construction of a vertically transversely isotropic (VTI) model and can be used to derive anisotropy parameters $(\epsilon, \delta, \gamma)$ and vertical velocities V_{P0} and V_{S0}. This process enables consistent upscaling of well-log elastic properties to the seismic resolution.

Appendix D. Model selection in copula models using information criteria

Selecting an appropriate copula model is a critical step in multivariate dependence modeling. The goal is to choose a model that either best fits the overall data structure or best estimates a parameter of specific interest. Classical model selection criteria such as the Akaike Information Criterion (AIC) and the Bayesian Information Criterion (BIC) are widely used for this purpose. These criteria are rooted in likelihood-based theory and offer a compromise between model fit and complexity. In the context of copula models, especially those estimated via pseudo-likelihood or two-stage maximum likelihood, the applicability and performance of these criteria must be carefully assessed.

Appendix D.1. Akaike information criterion (AIC).

The AIC is an estimator of the expected Kullback-Leibler distance between the true model and a candidate model (Claeskens and Hjort, 2008). In the context of copula models, when using a fully parametric formulation, the AIC can be expressed as:

$$\mathrm{AIC}=2(\ell_{n,\max}-p), \tag{D.1}$$

where $\ell_{n,\max}$ is the maximized likelihood function and p is the number of parameters in the model, including both marginal and copula parameters (Hofert et al., 2019).

This formulation remains valid for the pseudo-likelihood under the assumption that the full model, including the margins and copula, is parametric (Ko et al., 2019). In this case, the AIC can be reliably used for selecting among copula models.

Appendix D.2. Bayesian information criterion (BIC).

The BIC is derived from a Bayesian perspective and incorporates a stronger penalty for model complexity compared to AIC. It is defined as:

$$\mathrm{BIC}=2\ell(\widehat{\theta})-k\log(n), \tag{D.2}$$

where n is the sample size and k is the total number of parameters of both marginal and copula parameters (Claeskens and Hjort, 2008).

While BIC assumes that the true model is among the candidate models, it can be used for model selection in copula-based settings under similar assumptions as AIC. BIC may be particularly sensitive to the number of parameters in high-dimensional copula models, which can result in a preference for simpler structures.

References

Albert, J., 2009. Bayesian Computation with R (Use R!). Springer, New York.

Arreguin-Lopez, M.A., Reyna-Martinez, G., Sánchez-Hernández, H., Escamilla-Herrera, A., Gutierrez-Araiza, A., 2011. Tertiary Turbidite Systems in the Southwestern Gulf of Mexico. Geology.

Ausin, M.C., Lopes, H.F., 2010. Time-varying joint distribution through copulas. Comput. Stat. Data Anal. 54, 2383–2399. https://doi.org/10.1016/j.csda.2009.03.008.

Azevedo, L., Soares, A., 2017. Geostatistical Methods for Reservoir Geophysics. Springer International Publishing. https://books.google.fr/books?id=jShDgAAQBAJ.

Backus, G.E., 1962. Long-wave elastic anisotropy produced by horizontal layering. J. Geophys. Res. 67 (11), 4427–4440. https://doi.org/10.1029/JZ067i011p04427.

Bortoli, L.J., Alabert, F., Haas, A., Journel, A., 1993. Constraining Stochastic Images to Seismic Data. Springer.

Buland, A., Omre, H., 2003. Bayesian linearized AVO inversion. Geophysics 68, 185–198. https://doi.org/10.1190/1.1543206.

Bunks, C., Saleck, F.M., Zaleski, S., Chavent, G., 2012. Multiscale seismic waveform inversion. Geophysics 60 (5), 1457–1473. https://doi.org/10.1190/1.1443880.

Bárdossy, A., Li, J., 2008. Geostatistical interpolation using copulas. Water Resour. Res. 44 (7), W07412.. https://doi.org/10.1029/2007WR006115.

Chilès, J.P., Delfiner, P., 2012. Geostatistics: Modeling Spatial Uncertainty, second ed. Wiley Blackwell. https://doi.org/10.1002/9781118136188

Claeskens, G., Hjort, N.L., 2008. Model Selection and Model Averaging. Cambridge University Press. https://doi.org/10.1017/CBO9780511790485.

Cooke, D.A., Schneider, W.A., 1983. Generalized linear inversion of reflection seismic data. Geophysics 48, 665–676. https://doi.org/10.1190/1.1441497. https://pubs.geoscienceworld.org/geophysics/article-pdf/48/6/665/3114100/665.pdf.

Cosentino, L., 2001. Integrated reservoir studies. J. Chem. Inf. Model. 53. https://doi.org/10.1017/CBO9781107415324.004.

Deutsch, C.V., Journel, A.G., 1998. Gslib: Geostatistical Software Library and User's Guide. Springer, New York. https://doi.org/10.1016/0098-3004(94)90041-8.

Diaz-Viera, M., Anguiano-Rojas, P., Mousatov, A., Kazatchenko, E., Markov, M., 2006. Stochastic Modeling of Permeability in Double Porosity Carbonates Applying a Monte-Carlo Simulation Method with T-copulas. In: SPWLA 47th Annual Logging Symposium.

Diaz-Viera, M., Casar-González, R., 2005. Stochastic Simulation of Complex Dependency Pattern of Petrophysical Properties Using T-copulas. In: IAMG'05: GIS and Spatial Analysis.

Diaz-Viera, M., Erdely, A., Kerdan, T., Valle, R.D., Mendoza-Torres, F., 2017. Bernstein copula-based spatial stochastic simulation of petrophysical properties using seismic attributes as secondary variable. Geostatistics Valencia 2016, 487–504. https://doi.org/10.1007/978-3-319-46819-8_33.

Díaz-Viera, M.A., Le, V.H., Vázquez-Ramírez, D., 2021. Rgeoestad 2.0: Un Programa De Código Abierto Para Aplicaciones Geoestadísticas Basado En R-project. URL: https://github.com/esmg-mx/RGEOSTAD.

Doyen, P., 2007. Seismic Reservoir Characterization: an Earth Modelling Perspective. EAGE publications.. https://books.google.fr/books?id=Sy5QAQAAIAAJ

Dubrule, O., Exploration Geophysicists, S., Geoscientists, E.A., Engineers, 2003. Geostatistics for Seismic Data Integration in Earth Models: Distinguished Instructor Short Course. Society of Exploration Geophysicists. https://books.google.com.mx/books?id=Lc3Ehp0ULd8C.

Díaz-Viera, M.A., 2002. Geoestadística aplicada. Instituto de Geofísica 144. https://doi.org/10.1017/CBO9781107415324.004.

Erdely, A., Díaz-Viera, M.A., 2010. Nonparametric and semiparametric bivariate modeling of petrophysical porosity-permeability dependence from well log data. In: Jaworski, P., Durante, F., Härdle, W., Rychlik, T. (Eds.), Copula Theory and its Applications. Lecture Notes in Statistics, 198. Springer, Berlin, Heidelberg, pp. 267–278. https://doi.org/10.1007/978-3-642-12465-5_13.

Erdely, A., Díaz-Viera, M.A., 2015. A vine and gluing copula model for permeability stochastic simulation. In: Stochastic and Data Analysis Methods and Applications in Statistics and Demography, pp. 273–281. https://www.academia.edu/23463707/A_vine_and_gluing_copula_model_for_permeability_stochastic_simulation.

Fernandes, F.J.D., Teixeira, L., Freire, A.F.M., Lupinacci, W.M., 2024. Stochastic seismic inversion and bayesian facies classification applied to porosity modeling and igneous rock identification. Pet. Sci. 21, 918–935. https://doi.org/10.1016/j.petsci.2023.11.020.

de Figueiredo, L.P., Grana, D., Rodrigues, B.B., Emerick, A., 2025. Non-linear non-parametric geostatistical rock-physics inversion of elastic attributes for petrophysical properties using direct multivariate simulation. Comput. Geosci. 196, 105862. https://doi.org/10.1016/J.CAGEO.2025.105862.

Gelfand, V.A., Larner, K.L., 1984. Seismic lithologic modeling. Lead. Edge 3, 30–34. https://doi.org/10.1190/1.1439033.

Gnann, S.J., Allmendinger, M.C., Haslauer, C.P., Bárdossy, A., 2018. Improving copula-based spatial interpolation with secondary data. Spatial Statistics 28, 105–127. https://doi.org/10.1016/J.SPASTA.2018.07.001.

Grana, D., 2014. Probabilistic approach to rock physics modeling. Geophysics 79. https://doi.org/10.1190/geo2013-0333.1.

Grana, D., Fjeldstad, T., Omre, H., 2017. Bayesian Gaussian mixture linear inversion for geophysical inverse problems. Math. Geosci. 49, 493–515. https://doi.org/10.1007/s11004-016-9671-9.

Haas, A., Dubrule, O., 1994. Geostatistical inversion: A sequential method of stochastic reservoir modeling constrained by seismic data. First Break 12, 561–569.

Hernández-Maldonado, V., Díaz-Viera, M.A., Erdely, A., 2012. A joint stochastic simulation method using the bernstein copula as a flexible tool for modeling nonlinear dependence structures between petrophysical properties. J. Petrol. Sci. Eng. 90–91, 112–123. https://doi.org/10.1016/j.petrol.2012.04.018.

Hernández-Maldonado, V., Díaz-Viera, M.A., Erdely, A., 2014. A multivariate bernstein copula model for permeability stochastic simulation. Geofis. Int. 53, 163–181. https://doi.org/10.1016/S0016-7169(14)71498-9.

Hofert, M., Kojadinovic, I., Mächler, M., Yan, J., 2019. Elements of Copula Modeling with R. Springer International Publishing. https://books.google.com/books?id=QxyDDwAAQBAJ.

Joe, H., 2014. Dependence Modeling with Copulas. Taylor and Francis. https://books.google.com/books?id=09ThAwAAQBAJ.

Ko, V., Hjort, N.L., Haff, I.H., 2019. Focused information criteria for copulas. Scand. J. Stat. 46, 1117–1140. https://doi.org/10.1111/SJOS.12387.

Kohn, R., Pitt, M., Chan, D., 2006. Efficient bayesian inference for gaussian copula regression models. Biometrika 93, 537–554. https://doi.org/10.1093/biomet/93.3.537.

Le, V.H., 2021. Copula-based Modeling for Petrophysical Property Prediction Using Seismic Attributes as Secondary Variables. http://132.248.9.195/ptd2021/marzo/0810397/Index.html.

Le, V.H., Díaz-Viera, M.A., Vázquez-Ramírez, D., del Valle-García, R., Erdely, A., Grana, D., 2020. Bernstein copula-based spatial cosimulation for petrophysical property prediction conditioned to elastic attributes. J. Petrol. Sci. Eng. 193, 107382. https://doi.org/10.1016/j.petrol.2020.107382.

Liner, C.L., 2014. Long-wave elastic attenuation produced by horizontal layering. Lead. Edge 33, 634–638. https://doi.org/10.1190/tle33060634.1.

Min, A., Czado, C., 2010. Bayesian inference for multivariate copulas using pair-copula constructions. J. Financ. Econom. 8, 511–546. https://doi.org/10.1093/jfinec/nbp031.

Nelsen, R.B., 2006. In: An Introduction to Copulas, second ed. Springer, New York, NY, USA.

Oldenburg, D.W., Scheuer, T., Levy, S., 1983. Recovery of the acoustic impedance from reflection seismograms. Geophysics 48, 1318–1337. https://doi.org/10.1190/1.1441413.

Penna, R., Lupinacci, W.M., 2024. Geostatistical seismic inversion and 3D modelling of metric flow units, porosity and permeability in Brazilian presalt reservoir. Pet. Sci. 21, 1699–1718.. https://doi.org/10.1016/J.PETSCI.2024.02.013.

Pereira, A., Azevedo, L., Soares, A., 2023. Updating local anisotropies with template matching during geostatistical seismic inversion. Math. Geosci. 55, 497–519. https://doi.org/10.1007/s11004-023-10051-3.

Pereira, P., Calçôa, I., Azevedo, L., Nunes, R., Soares, A., 2020. Iterative geostatistical seismic inversion incorporating local anisotropies. Comput. Geosci. 24, 1589–1604. https://doi.org/10.1007/s10596-020-09966-1.

Pyrcz, M.J., Deutsch, C.V., 2014. Geostatistical Reservoir Modeling. OUP, USA.. https://books.google.com/books?id=wNhBAgAAQBAJ

Shemyakin, A., Kniazev, A., 2017. Introduction to Bayesian Estimation and Copula Models of Dependence. Wiley.. https://books.google.com/books?id=13gNDgAAQBAJ

Silva, R., Lopes, H., 2008. Copula, marginal distributions and model selection: a Bayesian note. Stat. Comput. 18, 313–320. https://doi.org/10.1007/s11222-008-9058-y.

Smith, M., 2011. Bayesian approaches to copula modelling. ERN: Bayesian Analysis (Topic). https://doi.org/10.2139/ssrn.1974297.

Trivedi, P., Zimmer, D., 2007. Copula modeling: An introduction for practitioners. Foundations and Trends(R) in Econometrics 1, 1–111. https://EconPapers.repec.org/RePEc:now:fnteco:0800000005.

Vázquez-Ramírez, D., 2018. Simulación Estocástica Conjunta De Propiedades Petrofísicas Con Cópulas De Bernstein Usando Atributos Sísmicos Como Variables Secundarias a Escala De Registros De Pozo. Universidad Nacional Autónoma de México. https://repositorio.unam.mx/contenidos/80610.

Vázquez-Ramírez, D., Huong Le, V., Díaz-Viera, M.A., del Valle-García, R., Erdely, A., 2023. Joint stochastic simulation of petrophysical properties with elastic attributes based on parametric copula models. Geofis. Int. 62, 487–506. https://doi.org/10.22201/igeof.2954436xe.2023.62.2.1593.

Zhang, Y., Yang, H., 2025. Direct inversion of 3D seismic reservoir parameters based on dual learning networks. Pet. Sci. 22 (10), 4037–4051. https://doi.org/10.1016/J.PETSCI.2025.05.027.